Green Chemistry

TUTORIAL REVIEW

View Article Online
View Journal | View Issue

Cite this: *Green Chem.*, 2024, **26**, 8564

Nonenzymatic ethanol production in sustainable ways

Lele Feng,[a,b] Jin Guo,[a,c] Jifeng Pang, *[a,b] Ming Yin,[a,b] Yujia Zhao,[a,b] Pengfei Wu[a] and Mingyuan Zheng *[a]

Received 1st April 2024,
Accepted 7th June 2024

DOI: 10.1039/d4gc01584c

rsc.li/greenchem

Ethanol is the most abundant chemical widely used in the fuel additive sector. Currently, it is mainly produced by the fermentation process, but it suffers from low carbon balance and poor reaction efficiency issues. In the past few decades, several promising catalytic methods have been proposed for ethanol production, depending on the available energy resources, technology development, and government policy. Herein, the catalytic pathways for ethanol production from petroleum, coal, natural gas, CO_2, and biomass in more sustainable ways are introduced. Specifically, the most crucial elementary steps in these catalytic pathways are reviewed and discussed, and key factors determining the feasibility of these catalytic reactions are listed, providing an all-around overview on the development of ethanol production in the near future. In the last section, an outlook was provided to highlight the challenges and opportunities for ethanol production and applications in more green and sustainable catalytic manners.

1. Introduction

Ethanol is the most historical organic compound involved in human evolution. In the Paleolithic or Neolithic period, ethanol was disclosed occasionally during the storage of fruits and then used as a main component in wine and a biological fluid for disease prevention.[1] In the 16th century, the term 'alcohol vini' was first used to name the spirit of wine by Paracelsus, and this name has remained since then.[2] In the 1800s, the chemical structure of ethanol was determined by the Scottish chemist Archibald Scott. During this period, the production of ethanol was less than 300 million gallons due to its limited applications in beverages, medicines, cosmetics and solvents.[3,4]

Since 1826, ethanol has been applied in internal combustion engines. Specifically, pure ethanol was first used as fuel in the automobile invented by Henry Ford in 1896. However, the demand for ethanol fuel fluctuated because of wars and governmental politics in different regions. At the beginning of the 20th century, cheap oil took over powering most nations, and ethanol languished in the fuel sector. During World War II, ethanol was revisited and blended with gasoline for use as an octane booster and fuel additive. After the war, the production of ethanol declined again owing to the limited extra demands. In the late 20th century, tetraethyl lead and methyl tertiary butyl ether (MTBE) were phased out of the octane booster list because of environmental issues caused by lead poisoning. Moreover, petroleum-based fuel became expensive owing to the "energy crisis", and stricter regulations were implemented to alleviate environmental concerns related to global warming. Along with the abundant carbohydrate feedstocks, the production of ethanol flourished and has been extensively applied in modern automobiles thanks to its high research octane number (RON = 109) and motor octane number (MON = 90).[5,6]

Owing to the abundant sugarcane resources as well as the good infrastructure and market, Brazil first initiated the National Alcohol Fuel Program (ProAlcool) to increase the production of bio-ethanol as a substitute for expensive gasoline, aiming to reduce the dependence on imported fossil fuel. With substantial government initiatives, ethanol has been used in vehicles mandatorily at a blend ratio larger than 20 v/v%. Although this decision was made by the government during a military regime, it was well accepted by civil society, agricultural farmers, and car manufacturers. Today, more than 90% of automobile production has flexible-fuel capability, consuming 7.42 billion gallons of ethanol in 2022.[7,8] Similarly, the dwindling fossil fuel resources and the increasing dependency of the United States of America (USA) on imported crude oil have also stimulated the exploration of large-scale ethanol production. Moreover, the replacement of toxic MTBE created an immediate ethanol demand of close to 3.5 billion gallons.[9] As the world's largest maize producer, corn in the U.S. Midwest has been selected for fermentation to produce ethanol. After the political incentive named "Biofuels

[a]*CAS Key Laboratory of Science and Technology on Applied Catalysis, Dalian Institute of Chemical Physics, Chinese Academy of Sciences, Dalian 116023, Liaoning, China. E-mail: jfpang@dicp.ac.cn, myzheng@dicp.ac.cn*
[b]*University of Chinese Academy of Sciences, Beijing 100049, China*
[c]*School of Materials Science and Engineering, Dalian Jiaotong University, Dalian, Liaoning 116028, China*

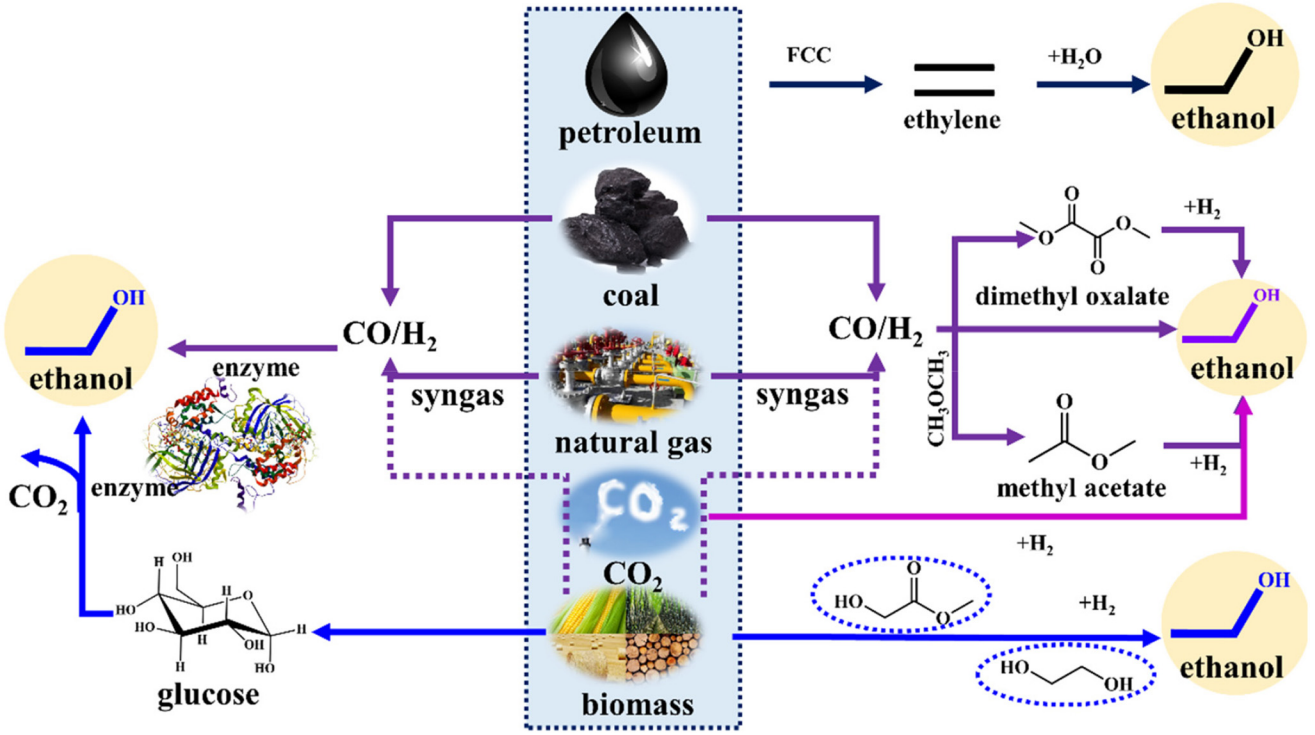

Fig. 1 Methods of ethanol production from petroleum, coal, natural gas, CO_2 and biomass (left and right pathways are biological and catalytic methods, respectively).

Initiative" in 2006, the production of ethanol in the USA reached 4.9 billion gallons, surpassing Brazil as the leading ethanol producer worldwide. Due to the mature fermentation and separation technologies, this number is continuously increasing and reached 17.3 billion gallons in 2020. Other regions, including the European Union, India, China, Canada, and Thailand, also set several goals to boost ethanol production. Nevertheless, due to the lack of cheap and abundant carbohydrates for fermentation and the emerging "food *vs.* fuel" debates, ethanol production in these regions is far below the demand. Thus, various strategies have been adopted to increase ethanol production from other energy resources.

At present, more than 80% of ethanol is produced by the fermentation technology. Nevertheless, this method is still facing several insurmountable obstacles. First and foremost, it is highly dependent on carbohydrate resources. As feedstock costs dominate the final ethanol price, the production of ethanol is mainly in sugarcane or corn-rich areas. Then, 2 moles of CO_2 are released during the fermentation of 1 mole of hexose with the maximum weight yield of ethanol of 51.1%. Finally, this process generally takes about 40–50 h with an ethanol productivity rate between 1 and 10 g L^{-1} h^{-1}, making it a low reaction efficiency process. Considering all these factors, some catalytic methods have been developed for ethanol production from petroleum, coal, natural gas, CO_2, and biomass. In the past few decades, great progress has been made for ethanol production in green and sustainable ways, even reaching the demonstration and/or industrial production scales (Fig. 1). Herein, thermal catalytic methods for ethanol production from petroleum, coal, natural gas, CO_2, and biomass are introduced. Then, the reaction processes and catalyst developments in different crucial steps are compared and discussed in more sustainable ways, trying to provide a holistic view of ethanol production in different regions. Finally, an outlook is presented to highlight the challenges and opportunities associated with ethanol production and consumption.

2. Catalytic methods for ethanol production

2.1 Hydration of petroleum-derived ethylene to ethanol

As an essential building block chemical, ethylene is mainly produced by the steam cracking of naphtha with an annual production greater than 200 million tons. Since the 1940s, it has been used as a feedstock for producing ethanol *via* the hydration reaction by Shell Chemicals. Afterwards, the fermentation process rapidly developed, making this process less economically feasible. Nevertheless, in some specific areas, such as the Middle East, the production of synthetic ethanol is growing due to the abundant ethylene and the shortage of agricultural products for fermentation.[10–12]

$$\begin{aligned} &CH_2{=}CH_2(g) + H_2O(g) \rightleftharpoons CH_3CH_2OH(g) \\ &\Delta H_{298} = -45.6\ \mathrm{KJ\ mol^{-1}} \end{aligned} \quad (1)$$

As shown in eqn (1), hydration of ethylene to ethanol is reversible and exothermic. This reaction is carried out at 500–573 K and 7–8 MPa with an ethylene to steam molar ratio of 0.6. Generally, the ethanol selectivity reaches 95–97% with *ca.* 95% unreacted ethylene recycled over acidic catalysts. Initially, a silica gel-supported phosphoric acid catalyst was utilized for this reaction by Shell. Then, great efforts have been made to replace this catalyst due to the environmental issues caused by the elimination of phosphorous compounds from catalysts under reaction conditions. A number of solid acid catalysts have been selected for this reaction. For instance, impregnated metal phosphates (metals: Ge, Zr, Ti, and Sn) were reported to have relatively high activities for the hydration of ethylene to ethanol. Additionally, some acidic zeolites and mixed oxides were also found to show high activities and selectivities.[13,14] In spite of this progress, the ethylene conversion is still very low, resulting in higher energy consumption and less economic competitiveness of this process. In contrast, great work has been done on the reverse reaction of ethanol dehydration to produce renewable ethylene due to the difficulty in ethylene production from raw biomass, continuous innovation in catalytic systems of Al_2O_3 and acidic zeolites, and abundant renewable ethanol supply in some areas, such as Brazil.[15,16]

2.2 Catalytic conversion of coal, natural gas and biomass-derived syngas into ethanol

Syngas, the short name for Synthetic Gas, is a mixture of carbon monoxide, hydrogen, and a small amount of impurities. Syngas is primarily produced through the thermochemical conversion of non-petroleum carbon resources, such as coal, natural gas, and biomass, and is used to generate electricity and produce a variety of key chemicals, such as ammonia, methanol, ethylene glycol, and hydrocarbons.[17–20] In detail, carbon resources such as coal react with oxygen obtained from the air separation unit to produce crude syngas at 1000–1270 K. Then, the H_2/CO ratio of syngas is adjusted by the water gas shift reaction, followed by the gas purification process to get syngas.[21] Considering the high energy consumption, environmental pollution issues and tremendous CO_2 emissions of this process, the carbon-neutral feedstock of biomass has been used to produce bio-syngas, aiming to reduce CO_2 emissions with a low carbon footprint.[22,23]

Thanks to the abundant syngas supply and the versatile application of ethanol, great efforts have been devoted to the conversion of syngas into ethanol. In the past decades, three different methods including direct conversion of syngas to ethanol, conversion of syngas to ethanol *via* the intermediate of dimethyl oxalate, and conversion of syngas to ethanol *via* the intermediate of acetic acid/methyl acetate have been developed for ethanol production, even on industrial scales.

2.2.1 Direct conversion of syngas into ethanol. The direct conversion of syngas into ethanol is the most attractive but challenging task for ethanol production (eqn (2)). Since the 1920s, this process has been hotly investigated along with the rapid development of methanol synthesis and Fischer–Tropsch synthesis (FTS) processes.[24] However, even after nearly one century of study, the conversion of CO and the selectivity to ethanol are still rather low, less than 40% and 10%, respectively, in most cases. The low ethanol selectivity is mostly attributed to the complex reaction networks, resulting in a variety of intermediates and by-products. As shown in Fig. 2, there are two kinds of CO adsorption approaches, *i.e.*, dissociated and non-dissociated adsorptions, depending on the active sites of catalysts. In the presence of surface adsorbed H*, the dissociated CO is hydrogenated to surface hydrocarbons (CHx*), which are reacted with the non-dissociated CO or C(H)O* species, and finally hydrogenated into ethanol. Besides this reaction pathway, the CHx* species are prone to hydrogenate into methane or couple and hydrogenate into C_{2+} hydrocarbons, and the C(H)O* species are apt to hydrogenate into methanol or couple and hydrogenate into C_{2+} oxygenates. Typically, the products follow the Anderson–Schulz–Flory (ASF) distribution due to the uncontrollable polymerization mechanism. Mathematically, the product distribution is depicted as a straight line plot of the logarithmic molar fraction *versus* the carbon number (slope is $\ln(\alpha)$, α indicates the chain growth probability).[25–27] According to the reaction mechanism, multiple active sites capable of dissociative and non-dissociative CO adsorption should be balanced and coupled to minimize side reactions, and correspondingly elevate the ethanol yield.[28–30]

$$2CO(g) + 4H_2(g) \rightleftharpoons CH_3CH_2OH(g) + H_2O(g)$$
$$\Delta H_{298} = -255.9\ \mathrm{KJ\ mol^{-1}} \quad (2)$$

After decades of exploration, four types of catalysts, *i.e.*, Rh-based catalysts, Mo-based catalysts, modified FTS catalysts, and modified methanol synthesis catalysts, have been developed for the direct conversion of syngas to ethanol.

Rh catalysts show excellent CO dissociation ability and moderate hydrogenation performances and have thus been used for the conversion of syngas to ethanol with the assistance of promoters. After screening the periodic table of elements, Fe, Mn, Li, Mo, and La were selected to modify Rh catalysts with appropriate metal–promoter interactions for higher ethanol yields.[31–34] Correlating with the reaction mechanism in Fig. 2, the presence of these metals creates

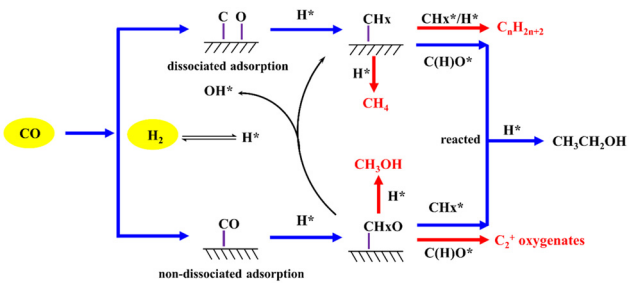

Fig. 2 Simplified reaction pathways for the direct conversion of syngas into ethanol (red lines indicated the main side reactions, * indicated the adsorbed state).

bifunctional active sites for CO adsorption or activation, facilitates the C(H)O species insertion, stabilizes the acetyl group and modifies the hydrogenation activity of catalysts. After minimizing side reactions, the selectivity to ethanol reached 50–75% at <10% CO conversions (unless noted otherwise, the selectivity and conversion were calculated on a carbon basis). Additionally, the productivity of ethanol was largely improved by adjusting the molar ratios of Rh^+ and Rh^0 or metal size distributions. For instance, intimate Rh^0–Rh^+–O–$Co^{\delta+}$ active sites were created over La–Rh–Co/ZrO_2 catalysts, which promoted CO dissociation and CO insertion, resulting in 55.7% selectivity to ethanol at 33.5% CO conversion.[35] Meanwhile, the combination of Rh single atoms and Rh nanoclusters with a ratio of 1 : 3 was found to promote ethanol selectivity and reaction rate over Rh/CeO_2 catalysts.[36]

Besides active metal sites, the catalyst preparation methods also tailored the geometric and electronic structures of Rh nanoparticles and affected the reaction results. For instance, encapsulating RhMn species into the CNTs boosted the ethanol productivity to 30.0 mol mol^{-1} Rh h^{-1}, more than an order of magnitude higher than that on the outside of the CNTs.[37] By controlling the interfaces between Rh and Mn, Rh species were anchored onto the Mn layer by the atomic layer deposition (ALD) method. This method promoted the C_{2+} oxygenate productivity more than the counterpart of Rh–Mn/SiO_2 catalysts but formed more acetaldehyde than ethanol due to the depressed hydrogenation activity.[38] Recently, the same RhMn sites were fixed within Silicate-1 (S-1) zeolite crystals for direct syngas conversion, and yielded 88.3% selectivity to C_2-oxygenate (mostly ethanol, with ethyl acetate and acetaldehyde as by-products) at 42.4% CO conversion (Fig. 3), much higher than most results in the literature. The Mn–O–$Rh^{\delta+}$ sites fixed within S-1 zeolite crystals not only boosted the ethanol production but also exhibited superior durability in the 220 h TOS (time on stream), providing a useful strategy for efficient catalyst design in syngas conversion.[39] In spite of these achievements, the relatively higher price of Rh, the low ethanol productivity, and the poor catalyst stability in most cases still restrict its applications on a large scale.

Since the 1980s, Mo-based catalysts have been widely investigated for the conversion of syngas into alcohols due to their abundant metal reserves, lower cost, CO_2 tolerance, and excellent sulfur-poisoning resistance properties. Different phases of Mo, including MoOx, MoS_2, Mo_2C, $MoSe_2$, and MoP, were selected as the active components for syngas conversions, and a series of metals were used to modify the Mo species for higher ethanol productivity.[40–45] Over the mostly investigated MoS_2 catalysts, the presence of alkali metals shifts the product from hydrocarbons to alcohols.[46] Metals of Co, Ni, Mn, La, and Rh have also been explored to modify the MoS_2 species for improved ethanol selectivity. For instance, the presence of Co created abundant Co–Mo–S phases with the assistance of K, which enhanced the CO non-dissociative adsorption, and subsequently promoted the CO insertion for high carbon alcohols formation.[47,48] Nevertheless, the produced mixed alcohols always follow the ASF distribution. As a main product, the ethanol selectivity is 10–40% in most cases.

FTS is the most well-known catalytic process for the conversion of syngas into hydrocarbon fuels since the 1920s. It follows a surface chain-growth mechanism, resulting in a distribution of hydrocarbons obeying ASF distribution over typical Co, Fe, or Ni catalysts.[49,50] To shift the product from hydrocarbons to alcohols, a second component, such as an alkali or transition metal, is always added to enhance the non-dissociative CO adsorption. After introducing Cu species, the formation of mixed Cu–Co alloy sites not only prevented Cu particle aggregation, but also boosted the selectivity to ethanol and C_{2+} alcohols.[51–53] Similarly, Cu was also selected to modify the Fe-based catalysts. By constructing the Cu–Fe(C) interfaces, the CO dissociation, non-dissociation and C–C bond propagation steps were improved and balanced to yield high carbon alcohols.[54] After immobilizing Fe_5C_2 clusters on the surface of Cu particles, the interfaces between Fe_5C_2 and Cu were maximized to obtain a space time yield of 0.101 g g_{cat}^{-1} h^{-1} for long-chain alcohols under a milder reaction pressure of 1 MPa.[55] Recently, hollow hydrophobic CuCoSNTs-c catalysts were synthesized for syngas conversion. The hydrophobic structure modulated the local microenvironment of CuCo sites *via* enriching CO and H_2 and repelling produced water, resulting in 28.2% selectivity to ethanol at 80.4% CO conversion in the 360 h TOS.[56] According to the FTS product of olefins, the reductive hydroformylation reaction was coupled for alcohol production. Over the mixed catalyst of NaOx/PrOx–CoRu/γ-Al_2O_3 + $Co_2(CO)_8$ with tricyclohexylphosphine ligands, the CO conversion and alcohol selectivity reached 34.0% and 53.7%, respectively, at 473 K, 12 MPa, and a H_2/CO ratio of 2.0, providing another option for alcohol productions.[57]

As early as the 1920s, methanol was produced catalytically from syngas at high temperatures (573–673 K) and pressures (25–35 MPa) over Cr_2O_3–ZnO catalysts.[58] Currently, the most widely used industrial catalyst is the Cu/ZnO/Al_2O_3 ternary composite regardless of the carbon resources (CO and/or CO_2). Under the mild conditions of 5–12 MPa and 503–553 K, methanol is industrially produced from syngas, with a global production of 110 million tons in 2022.[59,60] After changing catalyst preparation methods or adjusting Cu species, the main product shifts to ethanol *via* the synergy of Cu^+–Cu^0 and AlOOH active sites.[61] Additionally, large Cu particles with abundant Cu(111) facets and Cu(111)–ZnO interfaces weakened hydrogenation activity

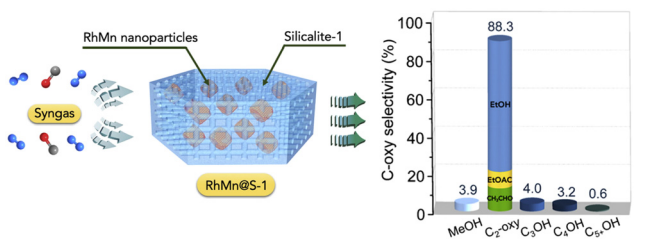

Fig. 3 The direct conversion of syngas to C_2-oxygenates over RhMn@S-1 catalysts (MeOH: methanol, EtOAC: ethyl acetate, and EtOH: ethanol).[39]

and facilitated CHx formation, resulting in an increased $C_{2+}OH$ selectivity of up to 68%.[62] In the following study, they also disclosed the crucial role of catalyst preparation methods in ethanol production, and further elevated the ethanol selectivity to >57% in ROH alcohols.[63–65] To further facilitate C–O bond scission and C–C coupling, the addition of transition metal/alkali–metal promoters is required for a higher ethanol selectivity. Typically, the productivity of C_{2+} alcohols was doubled in the presence of a cesium (Cs) promoter due to the synergistic effect among Cs, Cu, and ZnO components for the C–C bond coupling between CHx and CHyO species.[66]

To depress the catalyst deactivation issue stemming from the irreversible sintering of nanoparticles, phase separation or coking under harsh reaction conditions, great works have been done on encapsulating nanoparticles in zeolite, exposing specific facets for catalysis, or introducing additives to adjust the electronic structure or interaction of catalysts.[30,67–70] Additionally, shaping catalysts with binders is also indispensable for the industrial applications of catalysts. The binders shape the catalyst material into various morphologies and improve the mechanical strength of catalysts. However, in some cases, negative effects of binders on covering or modifying active sites also occurred.[71,72]

2.2.2 Catalytic conversion of syngas into ethanol *via* the intermediate of dimethyl oxalate. One of the indirect synthesis processes for the conversion of syngas to ethanol is through the intermediate of dimethyl oxalate (eqn (3)–(5)).[73] As shown in Fig. 4, CO is first coupled with alkyl nitrites (mostly methyl nitrite) to dimethyl oxalate and NO over Pd-based catalysts.[74] The second step is the hydrogenation of dimethyl oxalate to ethylene glycol with the co-produced methanol. The methanol is recycled back and reacted with NO in the presence of oxygen to methyl nitrite, and the ethylene glycol is hydrogenated to ethanol with the production of water. The first part for dimethyl oxalate production and the second part for the hydrogenation of dimethyl oxalate to ethylene glycol have been commercialized, especially in China, providing an attractive pathway for ethylene glycol production. However, in recent years, the textile industry has gradually transferred from China to Southeast Asia, and the demand for ethylene glycol gradually decreased, leading to the low price of ethylene glycol. In contrast, the ethanol market is very stable, and it is highly attractive for the conversion of dimethyl oxalate to ethanol in syngas-rich areas. In the first step, the dimethyl oxalate formation rate reached 899 g $(h\ L_{cat})^{-1}$ over 2–3 nm Pd catalysts. Although the ethanol production rates were slightly lower than the first step over typical Cu-based catalysts, this process is still reserved as a high efficiency process for the conversion of syngas to ethanol.[73] On the other side, this reaction is still facing several obstacles for applications, including low atom economy (produced water) and poor catalyst stability under harsh reaction conditions.

$$2CO + 1/2O_2 + 2CH_3OH \rightleftharpoons CH_3OCOCOOCH_3 + H_2O \quad (3)$$

$$CH_3OCOCOOCH_3 + 5H_2 \rightleftharpoons CH_3CH_2OH + 2CH_3OH + H_2O \quad (4)$$

Overall reaction:

$$2CO(g) + 1/2O_2(g) + 5H_2(g) \rightleftharpoons CH_3CH_2OH(g) + 2H_2O(g)$$
$$\Delta H_{298} = -497.7\ \mathrm{KJ\ mol^{-1}} \quad (5)$$

During the conversion of dimethyl oxalate to ethylene glycol, ethanol is also detected over Cu based catalysts. After modifying the reaction conditions, especially at higher temperatures, ethanol becomes the major product at the expense of ethylene glycol over the same Cu based catalysts. Generally, the reaction happens at 503–553 K, which is higher than the Hüttig temperature of metallic Cu. Thus, Cu catalysts are prone to deactivating through the migration and coalescence of particles. In the past decade, great works have been done intentionally for the conversion of dimethyl oxalate to ethanol. To meet the harsh reaction conditions, various strategies, including strong metal and support interactions, immobilizing metal particles inside the cavity, bimetallic catalysis, and metal oxide doping, have been dedicated to stable Cu particles for the conversion of dimethyl oxalate to ethanol (Fig. 5).[75] Over the Cu–SiO_2 catalyst prepared by the ammonia evaporation hydrothermal method, ethylene glycol is preferably produced at temperatures lower than 553 K, whereas at above 553 K the main product shifts to ethanol with a yield exceeding 80%. Due to the unique structure of catalysts and balanced Cu^+/Cu^0 species, the resulting Cu based catalysts ran for 200 h without any deactivation, providing an optional way for ethanol production from syngas.[73,76] After anchoring the Cu sites into the core (copper)–sheath (copper phyllosilicate) nanoreactor, the stability of Cu-phyllosilicate catalysts was largely improved in the 300 h TOS.[77] In other attempts, Cu nanoparticles were inlaid into mesoporous Al_2O_3, or mixed oxides of ZrO_2–Al_2O_3 and MgO–Al_2O_3, which created abundant metal–acid interfacial sites and balanced surface Cu^0–Cu^+ species, deserving >93% ethanol selectivity and >200 h stability.[78–80] Bimetallic catalysis is also an attractive way to adjust the stability and activity of Cu based catalysts. For instance, after introducing 1% Ni to Cu/SiO_2 catalysts, bimetallic Cu–Ni sites were formed to increase the metal surface

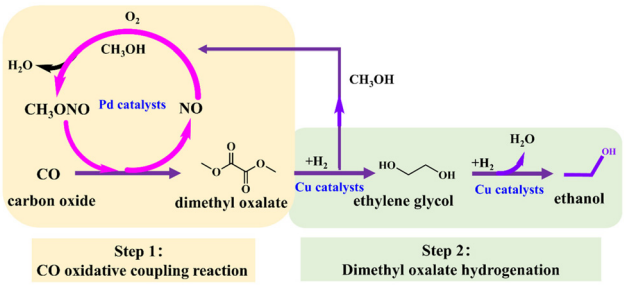

Fig. 4 Synthesis of ethanol from syngas *via* the intermediate of dimethyl oxalate.

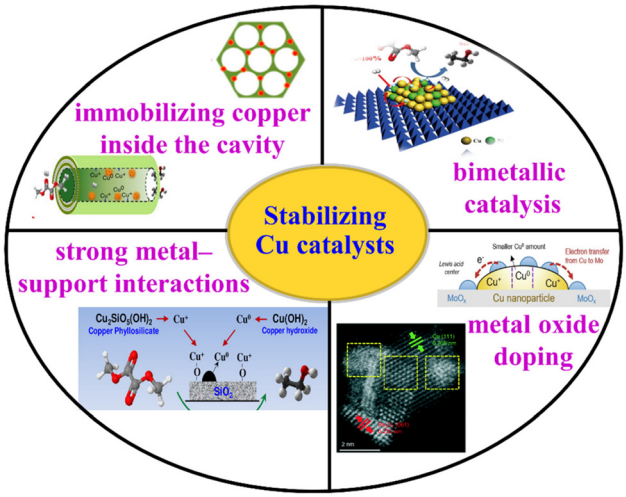

Fig. 5 Various strategies to stabilize Cu particles for ethanol production.[73,76,81,86]

areas and enhance the hydrogen chemisorption on the catalyst for the hydrogenation of dimethyl oxalate to ethanol.[81] To further improve the activity and stability of Cu based catalysts, a series of additives, including B, Zn, Ce, Re, and Mo, were introduced into Cu based catalysts to adjust the electronic interactions between metals, or balance the Cu^0/Cu^+ ratios, and subsequently yielded elevated dimethyl oxalate conversion and ethanol selectivity.[82–87]

Besides Cu based catalysts, some transition metal carbides also demonstrated high activity for the conversion of dimethyl oxalate to ethanol. Over the Mo_2C/SiO_2 catalyst, the ethanol selectivity reached 70.8% in the 350 h TOS at 543 K. Different from previous Cu based catalysts, methyl acetate is the key intermediate during the transformation process.[88] Similarly, the production of ethanol also goes through the intermediate of methyl acetate over an Fe_5C_2 nanocatalyst prepared by a precipitation method followed by carbonization in a methanol–H_2 mixture. Interestingly, the ethanol selectivity reached 89.6% at 533 K, much higher than that of the Mo_2C based catalyst.[89] When coupled with CuZnO–SiO_2 catalysts in a dual-bed configuration, the consecutive reactions were balanced, resulting in a low yield of by-products and a rather high ethanol yield of 98%.[90] Subsequently, a microsphere confined Fe@C catalyst was prepared for the hydrogenation of dimethyl oxalate. As shown in Fig. 6, ethanol was preferably produced with a yield as high as 84.3% at 543 K and a H_2/dimethyl oxalate molar ratio of 180. According to catalyst characterization, the Fe_5C_2 sites should play the key role in dimethyl oxalate hydrogenation into ethanol. Differently, methyl acetate was the main product (77.9%) at a low temperature of 513 K and a H_2/dimethyl oxalate molar ratio of 20 due to the changed active sites of Fe_3O_4.[91]

2.2.3 Catalytic conversion of syngas into ethanol *via* the intermediate of acetic acid/methyl acetate. Another indirect synthesis process for the conversion of syngas to ethanol is

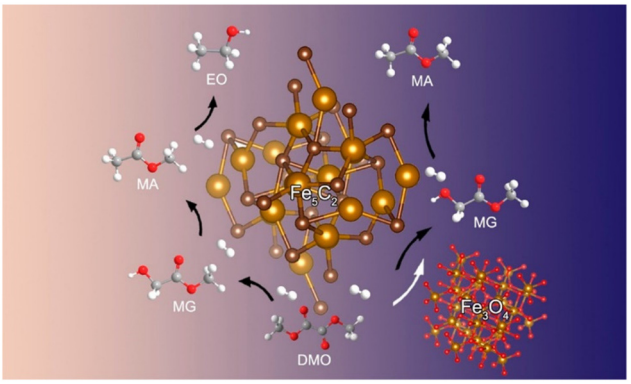

Fig. 6 Roles of different Fe species in dimethyl oxalate hydrogenation for ethanol production (DMO: dimethyl oxalate; MG: methyl glycolate; MA: methyl acetate; and EO: ethanol).[91]

through the intermediate of acetic acid/methyl acetate. As depicted in Fig. 7 and eqn (6)–(8) (dimethyl ether as the feedstock), syngas is first transformed into methanol over Cu/ZnO/Al_2O_3 catalysts. Then, the obtained methanol is directly converted into acetic acid *via* the methanol carbonylation process, or indirectly transformed into methyl acetate *via* the dehydration of methanol into dimethyl ether and the carbonylation of dimethyl ether to methyl acetate processes. Finally, the acetic acid or methyl acetate is hydrogenated into ethanol with the elimination of water or methanol.

$$CH_3OCH_3 + CO \rightleftharpoons CH_3COOCH_3 \quad (6)$$

$$CH_3COOCH_3 + 2H_2 \rightleftharpoons CH_3CH_2OH + CH_3OH \quad (7)$$

Overall reaction:

$$CH_3OCH_3(g) + CO(g) + 2H_2(g) \rightleftharpoons CH_3CH_2OH(g) + CH_3OH(g) \quad (8)$$
$$\Delta H_{298} = -142\ \mathrm{KJ\ mol^{-1}}$$

The carbonylation reaction is the most important and oldest reaction for the conversion of methanol or dimethyl ether into acetic acid and methyl acetate. In 1913, acetic acid was first synthesized as one of the main products from methanol and carbon monoxide (Fig. 8). Afterwards, iron, cobalt, and nickel (carbonyl) in the presence of an iodide salt were screened to convert methanol into acetic acid, even on an industrial level. Nevertheless, these reactions occurred under high pressures, but with a mediocre selectivity to acetic acid. In 1968, a breakthrough was achieved to obtain 99% acetic acid selectivity in a continuous process under mild conditions of 3 MPa and *ca.* 450 K, which was then named the Monsanto process. During this process, the active site of $[Rh(CO)_2I_2]^-$ is reacted with methyl iodide derived from methanol and a halide-bearing promoter to the intermediate of $[RhI_2(CH_3)(CO)_2]$, which is regarded as the rate-determining step for this reaction. Then, the I^- ligand is coordinated with the $[RhI_2(CH_3)(CO)_2]$ sites to the short-lived $[RhI_3(CH_3)(CO)_2]^-$ complex. Subsequently, CO is inserted in the Rh–CH_3 bond to

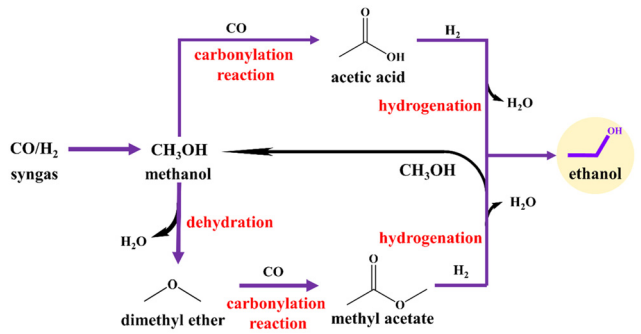

Fig. 7 Synthesis of ethanol from syngas *via* the intermediate of acetic acid/methyl acetate.

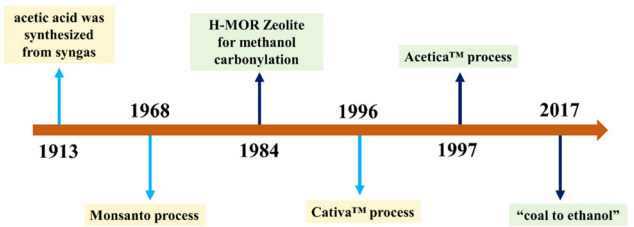

Fig. 8 The milestones for the conversion of syngas to ethanol *via* the intermediate of acetic acid/methyl acetate (from homogeneous to heterogeneous catalysts).

the thermodynamically preferred $[RhI_3(COCH_3)(CO)_2]^-$ complex. Finally, reductive elimination of CH_3COI occurs to yield acetic acid, HI and the active site of $[RhI_2(CO)_2]^-$.[92–94] In 1996, another impressive catalytic system named the Cativa™ process, *i.e.*, Ir species with CH_3I as the co-catalyst and Ru species as promoters, was exploited by the BP company. Due to the higher nucleophilicity of Ir species, the oxidative addition over $[IrI_2(CO)_2]^-$ sites to the $[IrI_2(CH_3)(CO)_2]$ complex is not the rate-determining step. In contrast, CO insertion into the neutral intermediate $[IrI_2(CH_3)(CO)_3]$ is the slowest step since it is 10^{-5} slower than that for Rh based catalysts. Afterwards, the $[IrI_2(CH_3)(CO)_3]$ site is transformed toward the $[IrI_2(COCH_3)(CO)_2]$ species, and then returned back to the initial site of $[IrI_2(CO)_2]^-$ sites with the release of acetic acid/methyl acetate.

Although the Monsanto and Cativa™ processes dominate the acetic acid market with an annual production of more than 18 million tons, great efforts have been made to heterogenize these homogeneous catalysts to avoid the complex separation procedures.[95] Some polymers are selected to graft the active sites of homogeneous catalysts for the carbonylation reaction. For instance, the $[RhI_2(CO)_2]^-$ complex is anchored on polyvinylpyridine resin, named the Acetica™ process, which demonstrated better Rh management than homogeneous alternatives.[96] Atomically dispersed Rh supported on porous organic polymers (POPs) also showed good performance for methanol carbonylation in the 400 h TOS.[97–99] In another attempt, single-site La–Ir based catalysts were also rather active and stable for vapor-phase methanol carbonylation.[100–102] Besides the Rh and Ir catalytic systems, Cu, Co, Ni, and Au species were also loaded on different supports for methanol carbonylation indispensable halide additives.[103–105] Recently, an attractive halide-free catalyst of atomically dispersed ReO_4 on SiO_2 was developed for acetic acid production. The obtained catalyst exhibited >93% selectivity in the 60 h TOS with a single pass methanol conversion >60%, providing a new class of potential methanol carbonylation catalyst.[106]

In 1984, Fujimoto *et al.* first disclosed the halide-free methanol carbonylation over mordenite (H-MOR) zeolites.[107] After introducing Cu species, the selectivity to acetic acid/methyl acetate was largely improved, reaching >70% in the 6 h TOS due to the preferential adsorption of CO and dimethyl ether on Cu species. However, the catalyst was deactivated rapidly with the main product shifting to dimethyl ether due to the blocked pores by polymethyl benzenes.[108]

Dimethyl ether is also a promising feedstock for carbonylation, as it can be readily produced by a simple methanol dehydration process catalyzed by solid acids such as alumina or zeolites, or directly produced from syngas.[109] Over the same H-MOR zeolite, the methyl acetate selectivity was boosted to 99% at temperatures <463 K using dimethyl ether as the feedstock. The Brønsted protons in zeolite provided suitable sites for dimethyl ether adsorption and CO insertion. Moreover, the anhydrous condition avoided the negative role of water in carbonylation pathways, resulting in a high carbonylation rate for methyl acetate production.[110] In the following research, H-MOR zeolites with 8-member ring (8-MR) channels were proved to be the active sites for dimethyl ether carbonylation, rather than zeolites without 8-MR channels such as H-BEA, H-FAU, H-MFI, and amorphous SiO_2–Al_2O_3 catalysts.[111] During this reaction, dimethyl ether is first adsorbed on Brønsted acid sites of 8-MR channels to methyl-saturated surfaces. Afterwards, the adsorbed CO is inserted into methoxy to produce the acetyl group, which is regarded as the rate-determining step in the whole elementary reaction. Finally, the acetyl group reacts with dimethyl ether to methyl acetate, resulting in the regeneration of methyl intermediates.[112–114] Under reaction conditions, the 8-MR channels in the H-MOR zeolite displayed obviously higher carbonylation activity, but the 12-MR channels caused carbon deposition, leading to the activity decrease and final complete deactivation. Thus, some studies tried to enhance the acid site in the 8-MR pore and reduce the acid site in the 12-MR pore for this reaction *via* enriching the Al location in the 8-MR pore during the catalyst synthesis procedures, or performing dealumination of the as-synthesized zeolite to relocate the Al atoms. Specifically, tailoring the Al atoms at the T3 and T4 sites over H-MOR zeolites was proved to be crucial for improved catalyst activity and stability, as evidenced by a combined approach of solid-state NMR experiments and DFT calculations.[115–117] Specifically, Xiong *et al.* found that the specific activity on the T3 site was 4 times that of the T4 site at 473 K. Over a plate-like H-MOR, 43% Al species were located on the T3 site, reserving

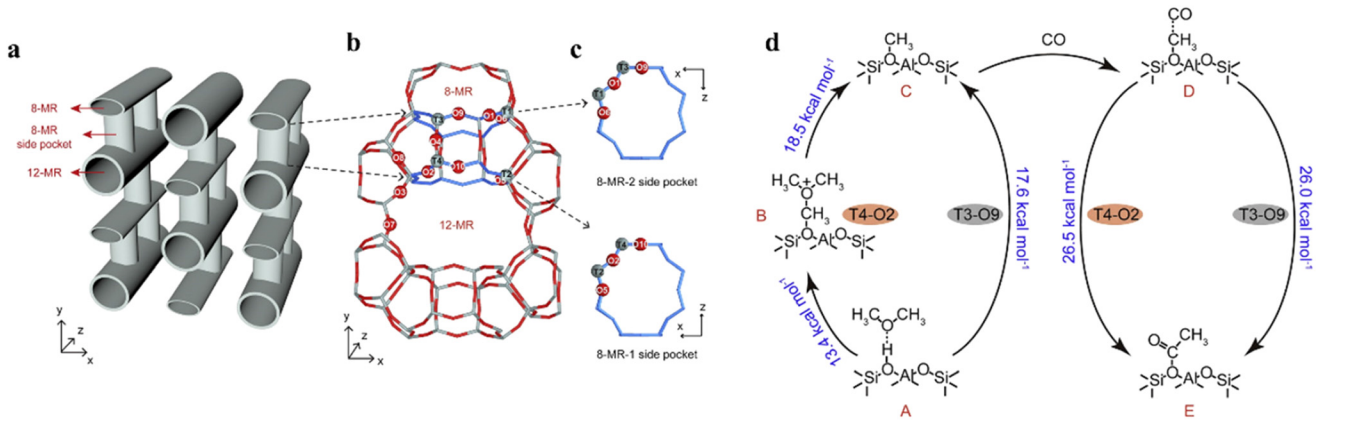

Fig. 9 The structure of the MOR zeolite: (a) the 12-MR and 8-MR pores connected *via* the 8-MR side pocket, (b) geometries of the T sites (T1–T4) and the O atoms (O1–O10), (c) schematic illustrations of the 8-MR side pocket viewed from the *y*/–*y* orientations, and (d) dimethyl ether dissociation and CO coupling with the surface methoxy group on the T3–O9 and T4–O2 sites.[117]

7.2 $mol_{methyl\ acetate}\ mol_{Al\text{-}T3}^{-1}\ h^{-1}$ under the reaction conditions of 473 K and 1.0 MPa (Fig. 9).[117] More attractively, pyridine was selected to adsorb on the acidic sites in the 12-MR pores to improve the stability of catalysts.[118] The pyridine molecules were found to be penetrated into 8-MR pockets and interacted with the Brønsted hydroxyls, and then desorbed preferentially after heating at 573–673 K. Over the pyridine treated H-MOR with a Si/Al ratio of 13.8, the methyl acetate yield reached 7.2 mmol $(g\ h)^{-1}$.[119] According to characterization, the adsorption of pyridine transformed the octahedrally coordinated Al species in H-MOR into typical high active tetrahedral coordination species, and thereby improved the catalyst stability and catalytic performance in the carbonylation of dimethyl ether to methyl acetate.[120,121] In the recent research by solid-state NMR spectroscopy, the CO carbonylation reaction occurred in the 8-MR pores of the pyridine treated H-MOR, while the methanol within the 12-MR was "locked" by the pyridine molecules to avoid the carbon–carbon coupling reactions.[122]

Another key step in ethanol production is the hydrogenation of acetic acid/methyl acetate. When using acetic acid as the feedstock, the typical catalysts are comprised of noble metals of group VIII and a second transition metal as the promoter dispersed on oxide supports.[45,123–125] Although most noble metal catalysts demonstrate good activity and ethanol selectivity, the limited resources and ever-growing price of noble metals greatly restrict their large-scale applications.[124] In the past decade, some organic acid-tolerant transition metal catalysts have been developed for acetic acid conversions, and also achieved rather good results. Due to the robust activity in C–O/C=O bond hydrogenation, Cu based catalysts have been used as the active site for acetic acid hydrogenation in the presence of different metal additives.[126–128] Typically, over 9Cu1In/SBA-15 catalysts, Cu–In alloys were formed to accelerate the dissociation of acetic acid to acetate and inhibit the combination of acetyl and ethoxy species to ethyl acetate, affording 99.1% acetic acid conversion and 90.9% selectivity to ethanol at 623 K in 2.5 MPa H_2.[129] Similarly, In or Sn was also used to modify Ni species for the conversion of acetic acid to ethanol, affording relatively high ethanol yields (for instance: 93% over the 4wt%Ni–4wt%Sn/TiO_2 catalyst at 473 K, 10 MPa H_2 and 12 h).[130,131]

For the hydrogenation of methyl acetate to ethanol, most researchers focus on Cu based catalysts due to the abundant reservation of Cu and the high activity for C=O bond hydrogenation. Over typical Cu based catalysts, Cu^0 sites split the gaseous H_2 into H*, and Cu^+ species activate the acyl species of methyl acetate. Then, the rate-determining step of acetyl hydrogenation happens to yield ethanol with the co-produced methanol for recycling.[132] Nevertheless, Cu particles are prone to aggregate under reaction conditions because of the low Tamman temperature and the metastability of Cu^+ species. To alleviate the deactivation of Cu catalysts, strong interactions between Cu species and supports were constructed for methyl acetate hydrogenation. For the benchmark Cu/SiO_2 catalyst, B, Ag, Ce, La, Mg, and Zn were added to improve the dispersion of Cu particles and inhibit particle aggregations.[133–137] Moreover, some novel strategies were employed to stabilize Cu catalysts. For instance, Cu species were confined in the support of CNTs, CeO_2, SBA-15 or mixed oxides, and yielded better performance and stability thanks to the increased Cu^0–$Cu^{\sigma+}$ interfaces.[138–140]

Recently, different functional catalysts were coupled for the conversion of syngas to ethanol. Over the relay catalysts of $ZnAl_2O_4$|H-MOR|$ZnAl_2O_4$, the elementary steps of converting syngas to dimethyl ether, carbonylation of dimethyl ether into methyl acetate, and hydrogenation of methyl acetate to ethanol were balanced, yielded 52% selectivity to ethanol at 6% CO conversion.[141] Afterwards, the same group developed a trifunctional tandem system composed of K-modified ZnO–ZrO_2, modified H-MOR zeolite, and Pt–Sn/SiC (Fig. 10, down), which catalyzed syngas conversion to methanol, methanol carbonylation, and acetic acid hydrogenation to ethanol, respectively. Over the optimized system, the ethanol selectivity reached 81% at 4.0% CO conversion in the 100 h TOS under the conditions of 543 K, H_2/CO = 1 : 1, and 5.0 MPa.[142] When

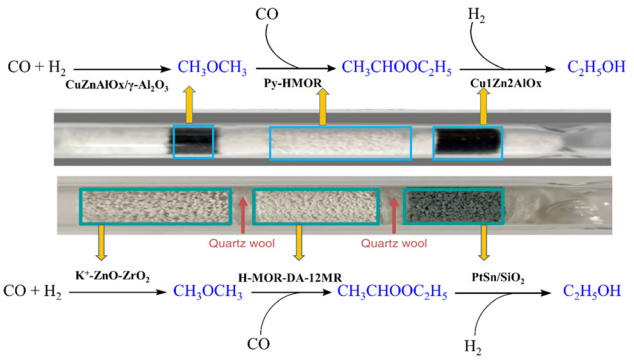

Fig. 10 Trifunctional tandem systems for the direct synthesis of ethanol from syngas (Py-HMOR and H-MOR-DA-12MR indicates the pyridine modified H-MOR and the H-MOR with selectively removed Al frameworks in the 12-MR channels, respectively).[142,144]

using methanol and syngas as the reactants, the H-MOR zeolite coated by the carbon layer and Pt–Sn/CNT catalysts afforded 60% selectivity to ethanol at 98% CH_3OH conversions.[143] In another attempt, a triple-tandem catalyst system consisting of CuZnAlOx/γ-Al_2O_3, pyridine modified H-MOR and Cu1Zn2AlOx was used to catalyze syngas into ethanol. As shown in Fig. 10 (up), after coupling the cascade reactions of syngas to ethyl ether, ethyl ether carbonylation to methyl acetate, and methyl acetate hydrogenation to ethanol, the ethanol selectivity reached 62% at 52% CO conversion with a high ethanol space–time yield of 6.5 mmol g^{-1} h^{-1}.[144]

By coupling the methanol or dimethyl ether carbonylation with the hydrogenation process, an indirect ethanol production pathway from syngas is formed. After overcoming the catalyst deactivation issues and scale-up problems, a coal to ethanol demonstration plant with a capacity of 100 000 metric tons per annum of ethanol was achieved with the cooperation of the Dalian Institute of Chemical Physics and Shaanxi Yanchang Petroleum Co., Ltd in 2017, and a larger industrial plant is under construction.[145] According to the life cycle analysis, the "coal to ethanol" process offers a feasible alternative for ethanol production because of its robust energy conservation effect and excellent economic competitiveness, but faces challenges of high CO_2 emissions.[146]

2.3 Catalytic conversion of CO_2 into ethanol

Due to the immoderate consumption of fossil energy sources, large amounts of CO_2 are emitted into the atmosphere, resulting in serious environmental issues such as global warming.[147] Besides being concentrated, pressurized, and stored during geological formation, CO_2 is also a useful energy carrier, especially with the renewable hydrogen produced by the electrolysis of water from solar energy.

$$2CO_2(g) + 6H_2(g) \rightleftharpoons CH_3CH_2OH(g) + 3H_2O(g)$$
$$\Delta H_{298} = -173.5\ \text{KJ mol}^{-1} \quad (9)$$

Among all the CO_2 utilization processes, hydrogenation of CO_2 into ethanol is of great significance (eqn (9)), but is scientifically challenging due to the thermodynamically stable and chemically inert properties of CO_2 and the high energy barrier of C–C bond formation.[148,149] In most cases, high CO_2 conversion and ethanol selectivity are difficult to achieve simultaneously due to the complex reaction pathways. As shown in Fig. 11, there are three proposed reaction mechanisms for the conversion of CO_2 to ethanol. During the RWGS + CO (RWGS: reverse water gas reaction) mediated mechanism, CO_2 is first hydrogenated to CO *via* the RWGS reaction. Then, CO is activated to *CO and further hydrogenated to *CHx for *CHx–*CO coupling. Similarly, the RWGS + CH_3OH mediated mechanism first transfers CO_2 to CO *via* the RWGS reaction, and then to adsorbed methanol and intermediates of *CHxO or CHx for coupling. Apart from the RWGS reaction, these two mechanisms are very similar to the direct pathway for converting syngas to ethanol. Differently, in the *HCOO mediated mechanism, CO_2 is directly hydrogenated to formate intermediates (*HCOO). Subsequently, the *HCOO species are hydrogenated to *CHx, and coupled with *HCOO to *CH_3COO for hydrogenation.[148]

Learning from the syngas to ethanol process, Rh, Co, and Cu based catalysts have been applied for the conversion of CO_2 to ethanol. In the 1990s, [$Rh_{10}Se$] supported on TiO_2 was found to be robust for ethanol production with a selectivity of up to 83%.[150] Over the Li modified Rh/SiO_2 catalyst, 15.5% ethanol selectivity and 7.0% CO_2 conversion were obtained at 513 K *via* the CO intermediate.[151] In the following study, RhFeLi/TiO_2 catalysts with abundant hydroxyls and Na–Rh@S-1 with embedded Na-promoted Rh nanoparticles demonstrated higher activity and selectivity toward ethanol for CO_2 hydrogenation.[67,152] Recently, Zheng *et al.* prepared a single-atom catalyst of Rh_1/CeTiOx for CO_2 hydrogenation into ethanol. At 523 K for 5 h, the ethanol selectivity reached 99.1% with a turnover frequency of 493.1 h^{-1}. According to the *in situ* DIRFTs and DFT calculations (Fig. 12), the oxygen-vacancy–Rh Lewis-acid–base pairs facilitated CO_2 adsorption and activation, and promoted the cleavage of CHxOH* and COOH* into CHx* and CO* species for coupling, leading to the remarkable high activity and selectivity to ethanol. Additionally, the strong Rh–O bond derived from Ti-doping-induced structural reconstruction provided improved catalytic stability.[153] In their subsequent study, Rh/CNP catalysts with

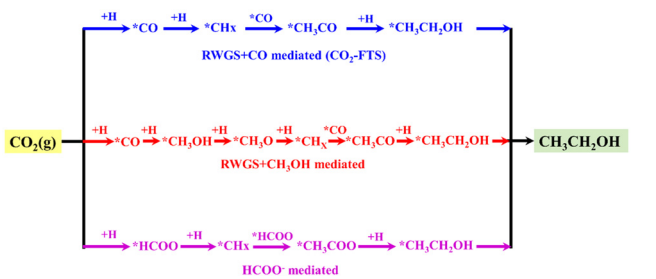

Fig. 11 Three reaction mechanisms for catalytic hydrogenation of CO_2 to ethanol (RWGS: reverse water gas reaction).[148]

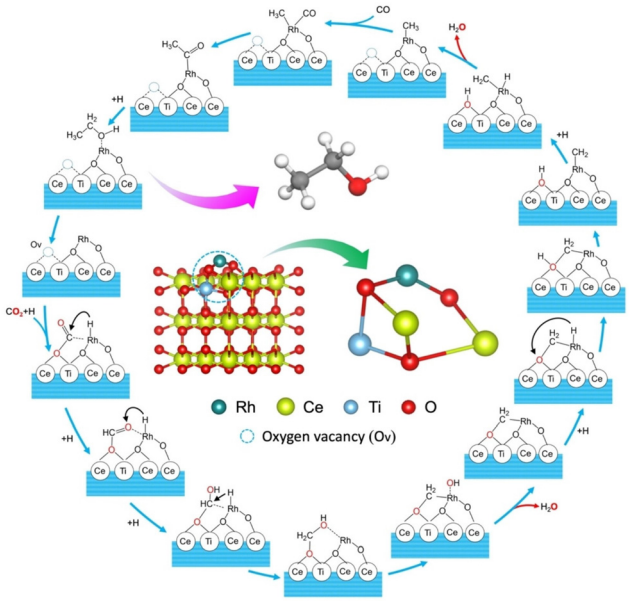

Fig. 12 The illustrated catalytic cycle of ethanol formation from CO_2 hydrogenation on the Rh_1/CeTiOx catalyst (the inset figure shows the structure of the Rh_1/CeTiOx catalyst).[153]

$Rh–N_3P_1$ sites were rationally synthesized for CO_2 conversion. The donation of electrons from P atoms effectively weakened the C–O bond in the intermediate of CH_3OH*, affording 81.8% ethanol selectivity at >69% CO_2 conversion.[154]

Due to the high activity in C–C coupling reactions, Co based catalysts were employed for CO_2 hydrogenations. For instance, Wang *et al.* prepared the CoAlOx catalyst from the Co–Al layered double hydroxide for CO_2 conversions. After adjusting the reduction temperature to 873 K, ethanol selectivity reached 92.1% at 413 K for 15 h.[155] Afterwards, they incorporated Ni species into the Co catalyst to boost the formation of relatively stable *CHx intermediates, resulting in 85.7% ethanol selectivity with 15.8 mmol g_{cat}^{-1} ethanol yield at 473 K for 12 h.[156] In another attempt, segregation of Co atoms was found to promote CO coverage, the C–O scission of $*CH_2O$ and C–C coupling, leading to >60% ethanol selectivity over the CoCu catalyst.[157] Nevertheless, the selectivity to ethanol is still very low over fixed-bed reactors. For instance, over Co/La_2O_3–$La_4Ga_2O_9$ catalysts, the CO_2 conversion and ethanol selectivity were 9.8% and 65.8% at 513 K with a GSHV (gas hourly space velocity) of 3000 mL $(g_{cat}\ h)^{-1}$.[158] Similarly, over Na–Co/SiO_2 and $CoGa_{1.0}Al_{1.0}O_4/SiO_2$ catalysts, the selectivity to ethanol was below 30% under different reaction conditions, even with the synergistic effect between Co^0 and $Co^{\delta+}$ species.[159–161]

In terms of Cu-based catalysts, multiple functional sites for $*CH_3$ and C–C bond formation should be constructed to yield C_{2+} alcohols. An *et al.* anchored Cu^I sites on a Zr_{12} cluster of a metal–organic framework (MOF) for hydrogenation of CO_2 to ethanol. Over the bimetallic Cu_2^I sites, H_2 was activated to $(Cu^{2+}–H^-)_2$ in the presence of alkali metal ions *via* bimetallic oxidative addition. Afterwards, CO_2 was inserted into methanol and formyl species. Then, a C–C bond was formed *via* a nucleophilic attack on the carbon of CH_3OH by a formyl group (CHO). Finally, the generated CH_3CHO was hydrogenated to ethanol with the return of Cu_2^I (M) sites. Over the Cs^+-modified MOF catalyst, >99% ethanol selectivity was obtained with a turnover number of 4080 in supercritical CO_2 (30 MPa CO_2 and 5 MPa H_2) at 358 K for 10 h.[162] As shown in Fig. 13, Ding *et al.* embedded 2–5 nm Cu nanoparticles in Na-beta zeolites for CO_2 hydrogenation in a traditional fixed-bed reactor, and yielded *ca.* 14% ethanol with a selectivity of nearly 100% at 573 K, 2.1 MPa and a space velocity of 12 000 mL $g_{cat}^{-1}\ h^{-1}$. The authors declared that CO_2 is first reacted with hydrogen to $*CH_3$ at the surface of Cu particles. Subsequently, the adsorbed $*CO_2$ is coupled with the produced $*CH_3$ to the key intermediate $*CH_3COO$. Finally, $*CH_3COO$ was hydrogenated to ethanol. Herein, the zeolitic framework confined and modulated the Cu nanoparticles with unique surface sites for the reactions. Also, it constrained the reactants at the layer nearby the nanoparticle surface to ethanol, rather than C_1 by-products.[163] Over the Cs-promoted Cu–Fe–Zn catalyst, Cs regulated the hydrogenation ability of CuFeZn catalysts for RWGS and CO insertion, Fe carbide and Cu species were responsible for CO dissociation and CO non-dissociative activation, respectively. The balance of different sites realized the high $C_{2+}OH/ROH$ fraction (93.8%) for CO_2 conversions.[164] During the study on methanol synthesis, Wang *et al.* disclosed the fine-tuning of *CHO species, which was used as the precursor to initiate the C–C coupling and the formation of ethanol *via* the key C_2-intermediate *OHCCHO over a Cu/Cs/ZnO(000$\bar{1}$) surface.[165]

Interestingly, some Pd, Au, and Ir based catalysts also demonstrated high activity in the conversion of CO_2 to ethanol. Bai *et al.* synthesized monodisperse Pd–Cu nanoparticles (NPs) by using a wet-chemical approach for CO_2 con-

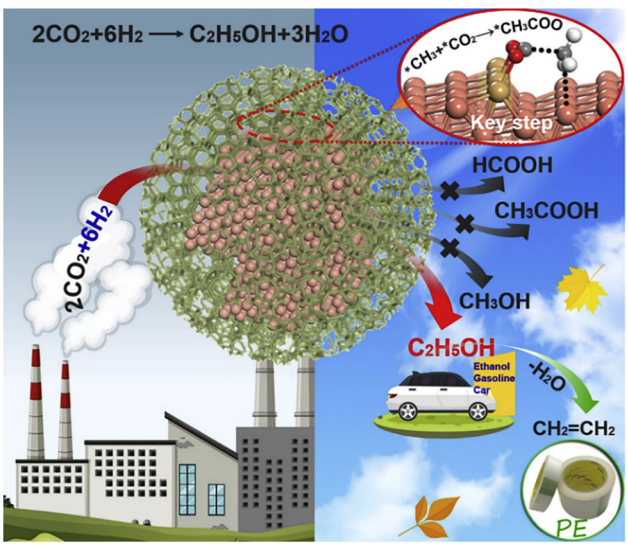

Fig. 13 Summary of the CO_2 hydrogenation to ethanol over the Cu@Na-Beta catalyst.[163]

version. Over the optimized catalyst of Pd_2Cu NPs/P_{25}, the ethanol selectivity reached 92% at 473 K for 5 h. According to DRIFTS experiments, the Pd–Cu alloy boosted the rate-determining step of *CO (adsorption CO) hydrogenation to *HCO, and then elevated the selectivity to ethanol.[166] Recently, Chen *et al.* achieved the conversion of CO_2 into the single-product of ethanol over a CeO_2-supported dual Pd site catalyst ($Pd_2Ce@Si_{16}$). The dual active sites of Pd showed extraordinary activity for the cleavage of the C–O bond in *CHxOH species and the C–C coupling between *CHx and *CO species. Additionally, the core–shell structure stabilized the Pd sites through enriching *in situ* formed water in the nanoreactor with a hydrophobic silica shell layer, leading to remarkably improved catalytic stability.[167] Thanks to the synergistic effect between Au nanoparticles and the TiO_2 support, >99% ethanol selectivity and 942.8 mmol g_{Au}^{-1} h^{-1} yield were achieved at 473 K for 10 h.[168] Yang *et al.* synthesized three non-metallic gold clusters of Au_9, Au_{11} and Au_{36} for CO_2 conversion. Different from Au_9 and Au_{36}, >80% selectivity to ethanol was obtained over Au_{11} catalysts due to the favoured CO*–CH_2* coupling.[169] Recently, Ye *et al.* loaded Ir single-atom on In_2O_3 for hydrogenation of CO_2 to ethanol. Over the bifunctional Ir_1–In_2O_3 catalyst, the Ir atom and the adjacent oxygen vacancy were coupled to a Lewis acid–base pair, which activated CO_2 to the intermediate species of carbonyl (CO*) adsorbed on the Ir atom ($Ir^{\delta+}$–CO*) and C–C coupling between CO* and CH_3O*, leading to a high ethanol selectivity of 99.7% at 473 K for 5 h.[170]

Besides the direct conversion of CO_2 to ethanol, some authors employed dimethyl ether or methanol and CO_2 for ethanol production *via* the methanol homologation process.[171–174] For instance, over Ru based catalysts with LiI as a promoter, the selectivity to ethanol in total products reached 71.7% at 453 K for 12 h.[158] When using 1-butyl-3-methylimidazolium chloride as the solvent, the reaction temperature decreased to 393 K.[172,174]

2.4 Catalytic conversion of biomass into ethanol

To solve the problems of low carbon balance and reaction efficiency in the fermentation process, great efforts have been devoted to the synthesis of ethanol *via* chemo-catalytic approaches from biomass. As the most abundant constituent of lignocellulosic biomass, cellulose is used as the feedstock for catalytic conversions by coupling the hydrolysis, C–C cleavage, and hydrodeoxygenation reactions.[175,176]

For the catalytic conversion of biomass to ethanol, the reaction pathways and intermediates are highly dependent on catalysts. Inspired by the one-pot conversion of cellulose to ethylene glycol process,[177–180] a two-step method was developed for the conversion of cellulose to ethanol. In the first step, WOx was used to selectively cleave the C–C bond of cellulose to methyl glycolate in the solvent of methanol and 1 MPa oxygen, achieving 57.7% methyl glycolate yield, even using raw cellulosic biomass such as birch, cornstalks, and miscanthus as feedstocks. Afterwards, methyl glycolate was hydrogenated to ethanol at a selectivity of 76.7% at 503 K over a 0.1Pt–Cu/SiO_2 single-atom alloy catalyst. By coupling the oxidation and hydrogenation steps, the indirect pathway for the conversion of cellulose into ethanol was achieved, as shown in Fig. 14.[181,182] In the following research, a one-pot process for the hydrogenation of cellulose into ethanol was achieved over a Mo–Pt/WOx catalyst. On this novel catalyst, xOMo–Pt–WOx interfacial sites were formed to catalyze the rate-determining step of hydrodeoxygenation of ethylene glycol to ethanol, resulting in 43.2% ethanol yield at 518 K for 2 h and a hydrogen pressure of 6 MPa.[183]

Simultaneously, Song *et al.* developed a binary catalytic system of H_2WO_4 and Pt/ZrO_2 for the direct conversion of cellulose into ethanol. Under reaction conditions, cellulose was hydrolyzed by the Brønsted acid sites in H_2WO_4 or the protons generated in high-temperature water. Then, the C–C bonds in the glucose unit were cleaved in the presence of H_2WO_4. Finally, the produced glycolaldehyde was converted into ethanol *via* the intermediate of ethylene glycol over Pt^0 and Pt^{2+} sites on Pt/ZrO_2 catalysts.[184] Li *et al.* designed a multifunctional Ru–WOx/HZSM-5 catalyst for the transformation of cellulose and raw biomass (bagasse and corn stalks) to ethanol. At 508 K for 20 h in 3 MPa hydrogen, the yields of ethanol reached 87.5% and 53.7%, respectively, for 1 wt% and 5 wt% cellulose conversions.[185] In another attempt, a binary catalyst of graphene-layer-encapsulated nickel (Ni@C) and H_3PO_4 was used to convert cellulose into ethanol. Unlike the previous intermediate of ethylene glycol, the cellulose was hydrolyzed into glucose and then interacted with H_3PO_4 to the cyclic diester for hydrogenolysis due to the synergistic effect between Ni@C and H_3PO_4. After optimizing the reaction conditions, a 69.1% yield of ethanol was obtained even at a final weight concentration of 8.9%, which is comparable to the value of fermentation processes.[186] In their following works, Co@C catalysts in the presence of H_3PO_4 and H_2WO_4 were also applied for cellulose conversion, and yielded 25.9% ethanol with ethylene glycol as the key by-product, indicating the key role of balanced metal and acid sites for ethanol production.[187,188]

Taking advantage of the robust C–C bond cleavage activity of W species, multiple functional catalysts were developed in the following years. For instance, Chu *et al.* developed a continuous process for the transformation of cellulose in corn stalk into ethanol. The corn stalk was first pretreated with 80% 1,4-butanediol to remove lignin. Then, the obtained cellulose

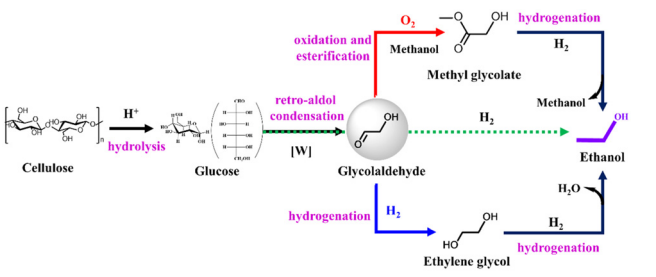

Fig. 14 One-pot and two-step reaction pathways for the conversion of cellulose into ethanol.

was converted into ethylene glycol over the 15%Ni–50%WOx/SiO_2 catalyst. Finally, the hydrogenolysis of ethylene glycol was conducted over the 1%Au–(20%Cu–2%Ni)/SiO_2 catalyst. After these cascade steps, the final ethanol yield reached 35.8% with a high weight concentration of 6.1% (ethanol in water).[189] Afterwards, they designed a multifunctional Pd–Cu–WOx/SiO_2 catalyst for the one-pot conversion of cellulose to ethanol, and yielded 42.5% ethanol after 10 h reaction at 573 K in the presence of 4 MPa H_2.[190] Similarly, Wu *et al.* employed Pt/WOx and Pt@HZSM-5 catalysts for the one-pot conversion of cellulose to ethanol. The encapsulation of Pt nanoparticles in the cavity of hollow HZSM-5 enhanced the activity for C–O cleavage of ethylene glycol, leading to an excellent ethanol yield of 54.4%.[191]

As shown in Fig. 15, the catalytic conversion of cellulose to ethanol is a cascade reaction with multiple side reactions, leading to a relatively low ethanol selectivity.[192,193] Under hydrothermal conditions, the hydrolysis of cellulose into glucose happens in the presence of *in situ* produced H^+ in water or solid acid catalysts. Then, the glucose was rapidly transformed into glycolaldehyde and hydrogenated to ethylene glycol. Otherwise, side reactions of glucose hydrogenation, isomerization and resinification occurred to produce a variety of side products. Finally, the produced ethylene glycol was converted into ethanol *via* the hydrogenolysis reaction. To achieve high ethanol yields, these steps should be balanced concisely, and side reactions with low energy barriers such as glucose and glycolaldehyde condensation, isomerization and direct hydrogenation reactions should be inhibited.

Different from other ethanol production pathways, the catalytic conversion of cellulose to ethanol is conducted under hydrothermal conditions, giving rise to great challenges in catalyst stability.[194,195] In the past decade, some attractive work has been done to improve the stability of catalysts *via* coating oxides or carbon layers, constructing strong metal–support interactions, embedding or anchoring metal particles, and employing bimetallic catalysts. For instance, alloys were formed to inhibit the leaching of Ni during the cellulose hydrolysis–hydrogenation process.[196,197] In another study, a high-loading (7.5 wt%) Ni–N–C single-atom catalyst was developed for cellulose hydrogenation, and it demonstrated unprecedented durability in the 7th recycle experiments at 518 K, 6 MPa H_2 in the presence of tungstic acid in hot water.[198]

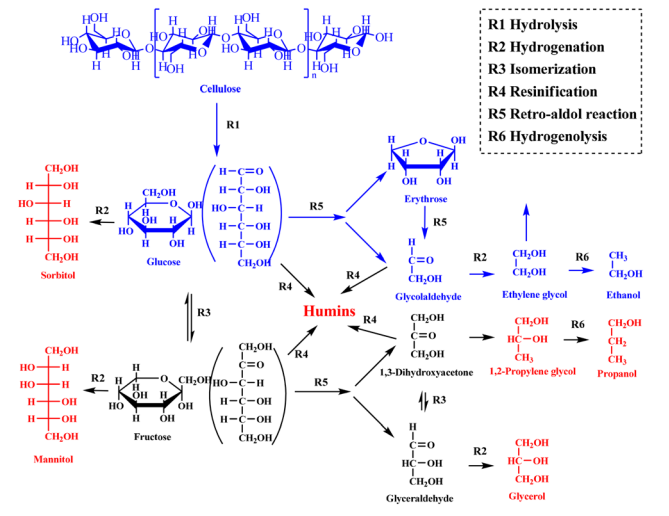

Fig. 15 Main and side reactions for the conversion of cellulose to ethanol (compounds in red are main by-products derived from side reactions).[176,180]

3. Summary and outlook

Due to the versatile application of ethanol in the chemical and fuel sectors, various methods have been explored for the production of ethanol from petroleum, coal, natural gas, CO_2, and biomass. As shown in Table 1, the key parameters for ethanol production from different feedstocks were listed and compared. The conversion of petroleum derived ethylene to ethanol is still feasible in some Middle-East areas. However, this process has the drawbacks of catalyst leaching issues and low reaction efficiency. The direct conversion of syngas to ethanol is a reaction with high atom economy but wide product distributions. In contrast, the indirect processes for ethanol production demonstrate high ethanol selectivity and reaction efficiency, showing high potential for applications. For instance, the "coal to ethanol" technology *via* the intermediate of methyl acetate has been operated at the industrial level in China. Recently, the direct conversion of CO_2 to ethanol has gained great attention. Although the ethanol selectivity surpassed 99% with considerable efficiency, the green hydrogen issues and low CO_2 conversion problems are yet to be resolved. The chemo-catalytic method for the transformation of biomass to ethanol is very promising, but still faces several challenges such as the reaction requiring to be conducted in an autoclave with solvents, and the resulting catalyst leaching. In future studies, more efforts should be emphasized on robust catalyst developments to improve ethanol selectivity and productivity. Moreover, process integration and energy-saving methods are encouraged to cut the energy consumption in ethanol production processes. Apart from the catalyst and reaction efficiency issues, the application of these methods is also highly dependent on the energy resources in the specific area. For instance, the "coal to ethanol" process is highly attractive in coal-rich areas, such as China. Additionally, government initiatives and carbon taxes also have profound impacts on the feasibility of different ethanol production pathways.[199] As discussed, the government initiatives boosted corn- or sugarcane-based ethanol production in the USA and Brazil. Similarly, the development of these newly emerged catalytic methods is also greatly affected by government initiatives such as subsidies, and zero-carbon industry incentives. Also, the carbon taxes will shift ethanol production to more sustainable methods, such as the direct conversion of cellulose to ethanol.

(1) Just a fuel additive? In the past decade, the production and application of pure electric vehicles have sharply increased

Table 1 Comparison of different catalytic reaction pathways for ethanol production[a]

Feedstock	Intermediate	Catalyst	Reaction conditions	Sel. (%)	Effi. (mmol h^{-1} g_{cat}^{-1})	Ref.
Ethylene	—	H_3PO_4/SiO_2	500–573 K, 7–8 MPa, ethylene/H_2O = 0.6	95–97	0.03–0.12	13
Syngas	—	RhMn@S-1	593 K, 3 MPa, H_2/CO = 2	88.3[b]	7.7	39
	—	K1.00–$MoSe_2$	593 K, 10.0 MPa, CO/H_2 = 1, GHSV = 3000 mL g^{-1} h^{-1}	31.1	1.2	44
	—	CuCoSNTs-c	543 K, 3 MPa, GHSV = 8000 h^{-1}, H_2/CO = 2/1	28.2	8.9	56
	—	CuZnAl	523 K, 4.0 MPa, GHSV = 450 mL g_{cat}^{-1} h^{-1}, H_2/CO = 2.0	14.2	0.2–0.5	62
	DMO	$Pd(111)/Al_2O_3$	403 K, 0.1 MPa, GHSV = 3000 h^{-1}	100	7.6[c]	74
		Cu/SiO_2	553 K, 2.5 MPa, LHSV = 2.0 h^{-1}, H_2/DMO = 200	83.0	5.6[c]	76
	Acetic acid	Rh or Ir complex	453 K, 3–4 MPa	>99	>1000[d]	92
		CuIn/SBA-15	623 K, 2.5 MPa H_2, LHSV = 1.25 h^{-1}	90.9	19.7[c]	129
	Methyl acetate	MOR zeolite	473 K, 2 MPa, GHSV = 3600 mL g^{-1} h^{-1}	>98	7.2	119
		Cu/ZnO–MgO	473 K, 5 MPa, LHSV = 1 h^{-1}	>86	7.96[c]	137
CO_2	—	Rh/CeTiOx	523 K, 3 MPa, 5 h (autoclave)	99.1	5.3	153
Cellulose	Methyl glycolate	WOx + CMK-3	513 K, 1 MPa O_2, methanol	55.7	24	181
		0.1Pt–Cu/SiO_2	503 K, 3 MPa, WHSV = 0.5 h^{-1}	76.7	5.2	182
	—	0.1Mo/2Pt/WOx	518 K, 6 MPa H_2, 2 h	43.2	5.4	183
		Ni@C-H_3PO_4	473 K, 5.5 MPa, 3 h	69.1	103	186

[a] Sel., Effi., Ref., GHSV, LHSV, and DMO are abbreviations for selectivity, efficiency, reference, gas hourly space velocity, liquid hour space velocity, and dimethyl oxalate, respectively. [b] The selectivity indicated the C_2-oxy in total oxygenates. [c] The unit is mol (L h)$^{-1}$. [d] Turnover frequency.

due to the higher well-to-wheel efficiency and available renewable electric power produced from water power, solar energy, and wind energy.[200–202] The shift from internal combustion engine vehicles to electric vehicles lowers the demand for fuels as well as fuel additives such as ethanol. In the near future, electric and internal combustion engine vehicles should coexist, and the demand for ethanol will be maintained at a moderate level. Considering the great amount of ethanol that has been produced and the possible reduced ethanol applications, it is highly desirable to upgrade ethanol to value-added chemicals, advanced fuels or materials such as hydrogen, butanol, aromatic compounds, aviation fuels and monomers that cannot be replaced by electric engines.[203–211]

(2) Homogeneous catalysts *vs.* heterogeneous catalysts. Homogeneous catalysts, usually organometallic complexes, generally demonstrate high activity, selectivity, and efficiency under mild reaction conditions. Carbonylation of methanol to acetic acid catalyzed by homogeneous Rh/Ir complexes is one of the most successful industrial applications, accounting for about 80% of acetic acid production worldwide.[212] Over the homogeneous Ir-based catalyst, the water level is reduced to <8% with a fast reaction efficiency and nearly 100% selectivity under mild reaction conditions. On the other hand, great efforts are devoted to developing heterogeneous catalysts due to product/catalyst separation issues. For instance, over the modified H-MOR catalyst, methyl acetate is produced from the gas-phase carbonylation of dimethyl ether, providing another option for C_2 compound production. Currently, both homogeneous and heterogeneous catalysts are running in industrial plants, and the feasibility of catalysts or processes is dependent on their economic and environmental impacts.

(3) Reaction mechanism study for novel catalytic system design. During all ethanol production processes, catalysts play a pivotal role in controlling product selectivity and reaction pathways. To design robust and stable catalysts, the reaction mechanism should be in-depth disclosed, and specifically the microenvironments between active sites and intermediates should be precisely controlled. In the past decades, a number of *operando* and *in situ* characterization methods, such as high resolution transmission electron microscopy, high-resolution synchrotron X-ray powder diffraction, and solid NMR have been developed to "see", "touch" and "feel" active sites and gain a deep understanding of catalysis. These results will provide solid guidance for novel catalyst design.[213] For instance, the in-depth understanding of the methanol carbonylation mechanism inspired the exploration of dual-ionically bound single-site rhodium catalysts for methanol carbonylation, resulting in a higher turnover frequency than Acetica and Monsanto processes.[97] Moreover, first-principles computations have been used to predict atomic-level details of catalytic reactions, providing promising guidance for the bottom-up design of novel heterogeneous catalysts at different nanoscales.[214]

(4) Balance different reaction steps. During most ethanol production processes, multiple steps should be subtly coupled and balanced. Taking the direct conversion of syngas or CO_2 to ethanol as an example, multiple sites for stabilizing CHx and C(H)O species should be coupled and balanced to promote the coupling of CHx and C(H)O species. Additionally, the kinetic study should be done to match each of the elementary steps. During the catalytic conversion of cellulose to ethanol, the rate of cellulose hydrolysis, C–C bond cleavage, and hydrodeoxygenation steps should be controlled to minimize side reactions. Otherwise, ethylene glycol or humins will dominate the product even over the same active site. Apart from the kinetic study, robust multiple functional catalysts are encouraged to be designed based on the interdisciplinary research between advanced materials, chemistry, physics, and engineering.

(5) Low carbon footprints of most processes. Regardless of feedstocks or reaction pathways for ethanol production, great

efforts have been made to minimize the energy consumption in a more environmentally friendly way. One method is to improve the product selectivity to lower separation energy consumption. For the direct conversion of syngas to ethanol, the elevated ethanol selectivity will largely reduce the energy for separation between ethanol and C_{2+} alcohols with similar properties. The other method is employing novel separation technology for ethanol production. Due to the azeotropic nature of the ethanol–water mixture, some hyperbranched polymers, molecular sieves and/or membranes are used to separate ethanol from the mixture in an energy-saving manner.[215–217] To achieve the goal of the Paris Agreement, great efforts have been made to employ renewable carbon and hydrogen resources for ethanol production. Through biomass gasification processes, renewable syngas is produced for the production of ethanol *via* direct or indirect routes.[218,219] Similarly, green hydrogen is produced by the electrolysis of water using solar energy. After integrating the hydrogenation processes, the carbon emissions of the whole ethanol production process will be largely reduced. Currently, according to the life cycle assessment analysis, the biochemical method for ethanol production shows better performance in terms of CO_2 emissions and fossil fuel consumption than the thermochemical conversion counterparts, such as syngas methods.[220–222] However, these differences will be decreased or diminished in the near future due to the improved ethanol yield, and scale effects, especially for some indirect pathways.

(6) Photocatalysis and electrocatalysis methods for ethanol synthesis. Under thermal catalytic reactions, cascade and parallel reactions co-happened to yield complex products with a low ethanol selectivity. To depress these side reactions, solar and/or electro-driven reactions have been extensively investigated and achieved great success. For instance, Cu–Ru-MOF hybrid materials with stable Cu^{I} species were synthesized for the conversion of CO_2 into ethanol under low-intensity light (450 LED, 11 mW cm^{-2}), yielding >99% selectivity to ethanol at 0.7% CO_2 conversion under the conditions of 423 K and 2 MPa of the H_2/CO_2 mixture (3 : 1).[223] In another attractive study, an ultra-stable gallium nitride semiconductor was developed for photo-driven one-step conversion of methanol to ethanol *via* the intermediate of methyl carbene, resulting in 0.5% volume of ethanol in methanol after 24 h reaction at 288 K with an impressive catalyst efficiency of 4050 μmol g^{-1} h^{-1}.[224] The electrochemical reduction of CO_2 to ethanol with renewable electricity represents a promising strategy to cut CO_2 emissions with green fuel production. To promote C–C bond formation, effective and stable Cu, Sn, and Ir based electrocatalysts were exploited for ethanol production.[225–228] Over SnS_2 nanosheets and single-Sn atoms anchored on three-dimensional carbon support catalysts, the C–C bond formation was promoted through a formyl-bicarbonate coupling pathway on dual active centers comprising Sn and O atoms, obtaining 82.5% selectivity to ethanol and 82.5% faradaic efficiency at −0.9 V_{RHE} and a geometric current density of 17.8 mA cm^{-2}.[229] Although the conversion of most C1 feedstock is very low, these methods still demonstrate great advantages, including high ethanol selectivity, low reaction temperature and pressure, and no limitation from thermodynamic equilibrium, providing high potential for further applications.

(7) "Ethanol economy" for carbon neutrality. Currently, ethanol is being used as a fuel additive to mitigate the problems associated with CO_2 emissions and fuel scarcity. With the rapid development of ethanol production *via* chemical pathways, the production of ethanol will be greatly increased in the near future. Correspondingly, the application of ethanol in the fuel and chemical sectors will also be greatly promoted. Similar to the concepts of methanol and hydrogen economies, these achievements will lead to the high feasibility of the "ethanol economy".[230,231] Additionally, the incorporation of renewable resources will reduce both the ethanol production cost and the overall environmental impact.[232] As the prevailing well-accepted fuel additive, ethanol has the potential to meet the energy demand with low carbon footprints.

Data availability

No primary research results, software or code have been included and no new data were generated or analysed as part of this review.

Conflicts of interest

The authors declare no conflict of interest.

Acknowledgements

This work was supported by the National Natural Science Foundation of China (22108274 and 22378383) and the "Transformational Technologies for Clean Energy and Demonstration", the Strategic Priority Research Program of the Chinese Academy of Sciences (XDA 21060200). Jifeng Pang would like to acknowledge the financial support provided by Shanxi Yanchang Petroleum (Group) Co., Ltd (yc-hw-2022ky-02). We also thank the anonymous reviewers for their constructive suggestions.

References

1 G. J. Soleas, E. P. Diamandis and D. M. Goldberg, *J. Clin. Lab. Anal.*, 1997, **11**, 287–313.
2 J. G. Ayres, *Br. J. Dis. Chest*, 1987, **81**, 80–86.
3 C. E. Wyman, in *Encyclopedia of Energy*, ed. C. J. Cleveland, Elsevier, New York, 2004, pp. 541–555. DOI: 10.1016/B0-12-176480-X/00518-0.
4 A. Devi, S. Bajar, P. Sihag, Z. U. D. Sheikh, A. Singh, J. Kaur, N. R. Bishnoi and D. Pant, *Bioengineered*, 2023, **14**, 81–112.
5 M. Balat and H. Balat, *Appl. Energy*, 2009, **86**, 2273–2282.

6 J. P. Szybist and D. A. Splitter, *Fuel*, 2018, **217**, 370–381.
7 J. Goldemberg, *Science*, 2007, **315**, 808–810.
8 M. L. Lopes, S. C. d. L. Paulillo, A. Godoy, R. A. Cherubin, M. S. Lorenzi, F. H. C. Giometti, C. D. Bernardino, H. B. d. Amorim Neto and H. V. d. Amorim, *Braz. J. Microbiol.*, 2016, **47**, 64–76.
9 D. Keeney, *Environ. Sci. Technol.*, 2009, **43**, 8–11.
10 F. J. Sanders and B. F. Dodge, *Ind. Eng. Chem.*, 1934, **26**, 208–214.
11 B. Roozbehani, M. Mirdrikvand, S. I. Moqadam and A. C. Roshan, *Chem. Technol. Fuels Oils*, 2013, **49**, 115–124.
12 A. Mohsenzadeh, A. Zamani and M. J. Taherzadeh, *ChemBioEng Rev.*, 2017, **4**, 75–91.
13 Y. Maki, K. Sato, A. Isobe, N. Iwasa, S. Fujita, M. Shimokawabe and N. Takezawa, *Appl. Catal., A*, 1998, **170**, 269–275.
14 N. Katada, Y. Iseki, A. Shichi, N. Fujita, I. Ishino, K. Osaki, T. Torikai and M. Niwa, *Appl. Catal., A*, 2008, **349**, 55–61.
15 M. Zhang and Y. Yu, *Ind. Eng. Chem. Res.*, 2013, **52**, 9505–9514.
16 B. Ma, L. Duan, Y. Ma, F. Bu, K. Lan, T. Zhao, L. Chen, L. Zu, L. Peng, Z. Zhao, J. Xu, S. Zhong, D. M. Aldhayan, A. M. Al-Enizi, A. Elzatahry, W. Li, W. Yang and D. Zhao, *Angew. Chem., Int. Ed.*, 2024, **63**, e202403245.
17 W. Zhou, K. Cheng, J. Kang, C. Zhou, V. Subramanian, Q. Zhang and Y. Wang, *Chem. Soc. Rev.*, 2019, **48**, 3193–3228.
18 C. J. R. Frazão and T. Walther, *Chem. Ing. Tech.*, 2020, **92**, 1680–1699.
19 Y. Liu, D. Deng and X. Bao, *Chem*, 2020, **6**, 2497–2514.
20 A. A. Tountas, G. A. Ozin and M. M. Sain, *Green Chem.*, 2021, **23**, 340–353.
21 D. Gao, X. Qiu, X. Zheng and Y. Zhang, *Chem. Eng. Res. Des.*, 2018, **131**, 709–722.
22 M. Bachmann, S. Völker, J. Kleinekorte and A. Bardow, *ACS Sustainable Chem. Eng.*, 2023, **11**, 5356–5366.
23 Y.-J. Chang, J.-S. Chang and D.-J. Lee, *Bioresour. Technol.*, 2023, **387**, 129535.
24 R. B. Anderson, J. Feldman and H. H. Storch, *Ind. Eng. Chem.*, 1952, **44**, 2418–2424.
25 J. Li, Y. He, L. Tan, P. Zhang, X. Peng, A. Oruganti, G. Yang, H. Abe, Y. Wang and N. Tsubaki, *Nat. Catal.*, 2018, **1**, 787–793.
26 T. Lin, Y. An, F. Yu, K. Gong, H. Yu, C. Wang, Y. Sun and L. Zhong, *ACS Catal.*, 2022, **12**, 12092–12112.
27 K. Cheng, Y. Li, J. Kang, Q. Zhang and Y. Wang, *Acc. Chem. Res.*, 2024, **57**, 714–725.
28 J. J. Spivey and A. Egbebi, *Chem. Soc. Rev.*, 2007, **36**, 1514–1528.
29 H. T. Luk, C. Mondelli, D. C. Ferré, J. A. Stewart and J. Pérez-Ramírez, *Chem. Soc. Rev.*, 2017, **46**, 1358–1426.
30 M. Ao, G. H. Pham, J. Sunarso, M. O. Tade and S. Liu, *ACS Catal.*, 2018, **8**, 7025–7050.
31 X. Mo, J. Gao, N. Umnajkaseam and J. G. Goodwin, *J. Catal.*, 2009, **267**, 167–176.
32 A. S. Asundi, A. S. Hoffman, P. Bothra, A. Boubnov, F. D. Vila, N. Yang, J. A. Singh, L. Zeng, J. A. Raiford, F. Abild-Pedersen, S. R. Bare and S. F. Bent, *J. Am. Chem. Soc.*, 2019, **141**, 19655–19668.
33 X. Huang, D. Teschner, M. Dimitrakopoulou, A. Fedorov, B. Frank, R. Kraehnert, F. Rosowski, H. Kaiser, S. Schunk, C. Kuretschka, R. Schlögl, M.-G. Willinger and A. Trunschke, *Angew. Chem., Int. Ed.*, 2019, **58**, 8709–8713.
34 P. Preikschas, M. Plodinec, J. Bauer, R. Kraehnert, R. Naumann d'Alnoncourt, R. Schlögl, M. Driess and F. Rosowski, *ACS Catal.*, 2021, **11**, 4047–4060.
35 Y. Mu, J. Zheng, Q. Yang, G. Liu, X. Liu, X. Wang, G. Wang, X. Liang and Y. Yuan, *ACS Appl. Nano Mater.*, 2023, **6**, 5692–5702.
36 D. Wu, S. Liu, M. Zhong, J. Zhao, C. Du, Y. Yang, Y. Sun, J. Lin, S. Wan, S. Wang, J. Huang, Y. Yao, Z. Li and H. Xiong, *ACS Catal.*, 2022, **12**, 12253–12267.
37 X. Pan, Z. Fan, W. Chen, Y. Ding, H. Luo and X. Bao, *Nat. Mater.*, 2007, **6**, 507–511.
38 N. Yang, J. S. Yoo, J. Schumann, P. Bothra, J. A. Singh, E. Valle, F. Abild-Pedersen, J. K. Nørskov and S. F. Bent, *ACS Catal.*, 2017, **7**, 5746–5757.
39 C. Wang, J. Zhang, G. Qin, L. Wang, E. Zuidema, Q. Yang, S. Dang, C. Yang, J. Xiao, X. Meng, C. Mesters and F.-S. Xiao, *Chem*, 2020, **6**, 646–657.
40 M. Xiang, D. Li, H. Xiao, J. Zhang, W. Li, B. Zhong and Y. Sun, *Catal. Today*, 2008, **131**, 489–495.
41 S. F. Zaman and K. J. Smith, *Catal. Today*, 2011, **171**, 266–274.
42 H. Shou, D. Ferrari, D. G. Barton, C. W. Jones and R. J. Davis, *ACS Catal.*, 2012, **2**, 1408–1416.
43 H. T. Luk, T. Forster, C. Mondelli, S. Siol, D. Curulla-Ferré, J. A. Stewart and J. Pérez-Ramírez, *Catal. Sci. Technol.*, 2018, **8**, 187–200.
44 H. Qu, S. He, Y. Su, Y. Zhang and H. Su, *Fuel*, 2020, **281**, 118760.
45 Z. Ren, Y. Cao, R. Cai, X. Dai, Y. Wei, F. Nie, X. Yin, Y. Gan, B. Wu, Y. Ye and X. Huang, *Chem. Eng. J.*, 2022, **440**, 135831.
46 X. Xiaoding, E. B. M. Doesburg and J. J. F. Scholten, *Catal. Today*, 1987, **2**, 125–170.
47 V. S. Dorokhov, E. A. Permyakov, P. A. Nikulshin, V. V. Maximov and V. M. Kogan, *J. Catal.*, 2016, **344**, 841–853.
48 H. Li, W. Zhang, Y. Wang, M. Shui, S. Sun, J. Bao and C. Gao, *J. Energy Chem.*, 2019, **30**, 57–62.
49 K. T. Rommens and M. Saeys, *Chem. Rev.*, 2023, **123**, 5798–5858.
50 Z. An, X. Ning and J. He, *J. Catal.*, 2017, **356**, 157–164.
51 G. Prieto, S. Beijer, M. L. Smith, M. He, Y. Au, Z. Wang, D. A. Bruce, K. P. de Jong, J. J. Spivey and P. E. de Jongh, *Angew. Chem., Int. Ed.*, 2014, **53**, 6397–6401.
52 W. Gao, Y. Zhao, H. Chen, H. Chen, Y. Li, S. He, Y. Zhang, M. Wei, D. G. Evans and X. Duan, *Green Chem.*, 2015, **17**, 1525–1534.
53 Z. Li, G. Luo, T. Chen, Z. Zeng, S. Guo, J. Lv, S. Huang, Y. Wang and X. Ma, *Fuel*, 2020, **278**, 118292.

54 Y. Lu, R. Zhang, B. Cao, B. Ge, F. F. Tao, J. Shan, L. Nguyen, Z. Bao, T. Wu, J. W. Pote, B. Wang and F. Yu, *ACS Catal.*, 2017, **7**, 5500–5512.
55 Y. Li, W. Gao, M. Peng, J. Zhang, J. Sun, Y. Xu, S. Hong, X. Liu, X. Liu, M. Wei, B. Zhang and D. Ma, *Nat. Commun.*, 2020, **11**, 61.
56 G. Chen, O. A. Syzgantseva, M. A. Syzgantseva, L. Peng, D. Stoian, M. Li, I. Akpinar, G. Yan, T. Xue, Q. Lyu, Z. Wang, T. Lei, X. Zeng, L. Lin and S. Yang, *Appl. Catal., B*, 2023, **334**, 122840.
57 K. Jeske, T. Rösler, M. Belleflamme, T. Rodenas, N. Fischer, M. Claeys, W. Leitner, A. J. Vorholt and G. Prieto, *Angew. Chem., Int. Ed.*, 2022, **61**, e202201004.
58 M. Bowker, *ChemCatChem*, 2019, **11**, 4238–4246.
59 M. Behrens, F. Studt, I. Kasatkin, S. Kühl, M. Hävecker, F. Abild-Pedersen, S. Zander, F. Girgsdies, P. Kurr, B.-L. Kniep, M. Tovar, R. W. Fischer, J. K. Nørskov and R. Schlögl, *Science*, 2012, **336**, 893–897.
60 Y.-F. Shi, P.-L. Kang, C. Shang and Z.-P. Liu, *J. Am. Chem. Soc.*, 2022, **144**, 13401–13414.
61 Y. Gu, C. Han, J. Huang, V. A. Vinokurov and W. Huang, *Fuel*, 2022, **322**, 124111.
62 Y. Liu, Z. Li, P. Luo, N. Cui, K. Wang and W. Huang, *Appl. Catal., B*, 2023, **336**, 122949.
63 J. Liu, J. Fan, F. Li, J. Gong, S. Wang, D. Yang and W. Huang, *ChemCatChem*, 2022, **14**, e202101848.
64 P. Jia, Y. Liu, R. Yang, P. Luo and W. Huang, *Fuel*, 2022, **323**, 124265.
65 S. Wang, J. Liu, J. Gong, Q. Guo, J. Fan and W. Huang, *J. Phys. Chem. C*, 2023, **127**, 11046–11057.
66 J. Sun, Q. Cai, Y. Wan, S. Wan, L. Wang, J. Lin, D. Mei and Y. Wang, *ACS Catal.*, 2016, **6**, 5771–5785.
67 F. Zhang, W. Zhou, X. Xiong, Y. Wang, K. Cheng, J. Kang, Q. Zhang and Y. Wang, *J. Phys. Chem. C*, 2021, **125**, 24429–24439.
68 T. Lin, F. Yu, Y. An, T. Qin, L. Li, K. Gong, L. Zhong and Y. Sun, *Acc. Chem. Res.*, 2021, **54**, 1961–1971.
69 A. J. Martín, S. Mitchell, C. Mondelli, S. Jaydev and J. Pérez-Ramírez, *Nat. Catal.*, 2022, **5**, 854–866.
70 J. Huang, K. Bai, M. Gao and W. Huang, *Int. J. Hydrogen Energy*, 2023, **48**, 33850–33863.
71 N.-L. Michels, S. Mitchell and J. Pérez-Ramírez, *ACS Catal.*, 2014, **4**, 2409–2417.
72 J. Lu, S. Wang, Y. Hao, L. Lin, F. Bai, W. Cui, J. Wang, Q. An, P. Tian, J. Pang and W. Luo, *Catal. Commun.*, 2024, **187**, 106892.
73 H. Yue, X. Ma and J. Gong, *Acc. Chem. Res.*, 2014, **47**, 1483–1492.
74 Z.-N. Xu, J. Sun, C.-S. Lin, X.-M. Jiang, Q.-S. Chen, S.-Y. Peng, M.-S. Wang and G.-C. Guo, *ACS Catal.*, 2013, **3**, 118–122.
75 R.-P. Ye, L. Lin, L.-C. Wang, D. Ding, Z. Zhou, P. Pan, Z. Xu, J. Liu, H. Adidharma, M. Radosz, M. Fan and Y.-G. Yao, *ACS Catal.*, 2020, **10**, 4465–4490.
76 J. Gong, H. Yue, Y. Zhao, S. Zhao, L. Zhao, J. Lv, S. Wang and X. Ma, *J. Am. Chem. Soc.*, 2012, **134**, 13922–13925.
77 H. Yue, Y. Zhao, S. Zhao, B. Wang, X. Ma and J. Gong, *Nat. Commun.*, 2013, **4**, 2339.
78 Y. Zhu, X. Kong, X. Li, G. Ding, Y. Zhu and Y.-W. Li, *ACS Catal.*, 2014, **4**, 3612–3620.
79 Y. Zhu, X. Kong, S. Zhu, F. Dong, H. Zheng, Y. Zhu and Y.-W. Li, *Appl. Catal., B*, 2015, **166–167**, 551–559.
80 G. Cui, X. Meng, X. Zhang, W. Wang, S. Xu, Y. Ye, K. Tang, W. Wang, J. Zhu, M. Wei, D. G. Evans and X. Duan, *Appl. Catal., B*, 2019, **248**, 394–404.
81 Y. Zhao, S. Zhao, Y. Geng, Y. Shen, H. Yue, J. Lv, S. Wang and X. Ma, *Catal. Today*, 2016, **276**, 28–35.
82 S. Zhao, H. Yue, Y. Zhao, B. Wang, Y. Geng, J. Lv, S. Wang, J. Gong and X. Ma, *J. Catal.*, 2013, **297**, 142–150.
83 M. Abbas, J. Zhang, Z. Chen and J. Chen, *New J. Chem.*, 2018, **42**, 17553–17562.
84 P. Ai, M. Tan, P. Reubroycharoen, Y. Wang, X. Feng, G. Liu, G. Yang and N. Tsubaki, *Catal. Sci. Technol.*, 2018, **8**, 6441–6451.
85 Z. Du, M. Chen, X. Wang, X. Chen, X. Mou, Y. Tan, W. Yang, C. Huang, H. Zhu, R. Lin and Y. Ding, *Catal. Sci. Technol.*, 2020, **10**, 3175–3180.
86 Z. Du, Z. Li, S. Wang, X. Chen, X. Wang, R. Lin, H. Zhu and Y. Ding, *J. Catal.*, 2022, **407**, 241–252.
87 Z. Li, Y. Li, X. Wang, Y. Tan, W. Yang, H. Zhu, X. Chen, W. Lu and Y. Ding, *Chem. Eng. J.*, 2023, **454**, 140001.
88 Y. Liu, J. Ding, J. Sun, J. Zhang, J. Bi, K. Liu, F. Kong, H. Xiao, Y. Sun and J. Chen, *Chem. Commun.*, 2016, **52**, 5030–5032.
89 J. He, Y. Zhao, Y. Wang, J. Wang, J. Zheng, H. Zhang, G. Zhou, C. Wang, S. Wang and X. Ma, *Chem. Commun.*, 2017, **53**, 5376–5379.
90 X. Shang, H. Huang, Q. Han, Y. Xu, Y. Zhao, S. Wang and X. Ma, *Chem. Commun.*, 2019, **55**, 5555–5558.
91 Y. Sun, Q. Ma, Q. Ge and J. Sun, *ACS Catal.*, 2021, **11**, 4908–4919.
92 P. Kalck, C. Le Berre and P. Serp, *Coord. Chem. Rev.*, 2020, **402**, 213078.
93 S. A. Fors and C. A. Malapit, *ACS Catal.*, 2023, **13**, 4231–4249.
94 A. Haynes, in *Adv. Catal*, ed. B. C. Gates and H. Knözinger, Academic Press, 2010, vol. 53, pp. 1–45.
95 Z. Ren, Y. Lyu, X. Song and Y. Ding, *Appl. Catal., A*, 2020, **595**, 117488.
96 Y. Noriyuki, M. Takeshi, W. Joe and S. Ben, in *Stud. Surf. Sci. Catal*, ed. H. Hattori and K. Otsuka, Elsevier, 1999, vol. 121, pp. 93–98.
97 Z. Ren, Y. Lyu, X. Song, Y. Liu, Z. Jiang, R. Lin and Y. Ding, *Adv. Mater.*, 2019, **31**, 1904976.
98 Z. Ren, Y. Liu, Y. Lyu, X. Song, C. Zheng, S. Feng, Z. Jiang and Y. Ding, *J. Catal.*, 2019, **369**, 249–256.
99 S. Feng, J. Mu, X. Lin, X. Song, S. Liu, W. Shi, W. Zhang, G. Wu, Y. Jiayue, W. Dong, X. Yang, J. Li, Z. Jiang and Y. Ding, *Appl. Catal., B*, 2023, **325**, 122318.
100 J. H. Kwak, R. Dagle, G. C. Tustin, J. R. Zoeller, L. F. Allard and Y. Wang, *J. Phys. Chem. Lett.*, 2014, **5**, 566–572.

101 A. J. R. Hensley, J. Zhang, I. Vinçon, X. Pereira Hernandez, D. Tranca, G. Seifert, J.-S. McEwen and Y. Wang, *J. Catal.*, 2018, **361**, 414–422.
102 Z. Ren, Y. Lyu, S. Feng, X. Song and Y. Ding, *Chin. J. Catal.*, 2018, **39**, 1060–1069.
103 A. Goguet, C. Hardacre, I. Harvey, K. Narasimharao, Y. Saih and J. Sa, *J. Am. Chem. Soc.*, 2009, **131**, 6973–6975.
104 F. Pang, F. Song, Q. Zhang, Y. Tan and Y. Han, *Chem. Eng. J.*, 2016, **293**, 129–138.
105 F. Li, J. Huang, J. Zou, P. Pan and G. Yuan, *Appl. Catal., A*, 2003, **251**, 295–304.
106 J. Qi, J. Finzel, H. Robatjazi, M. Xu, A. S. Hoffman, S. R. Bare, X. Pan and P. Christopher, *J. Am. Chem. Soc.*, 2020, **142**, 14178–14189.
107 K. Fujimoto, T. Shikada, K. Omata and H. Tominaga, *Chem. Lett.*, 1984, **13**, 2047–2050.
108 T. Blasco, M. Boronat, P. Concepción, A. Corma, D. Law and J. A. Vidal-Moya, *Angew. Chem., Int. Ed.*, 2007, **46**, 3938–3941.
109 J. Sun, G. Yang, Y. Yoneyama and N. Tsubaki, *ACS Catal.*, 2014, **4**, 3346–3356.
110 P. Cheung, A. Bhan, G. J. Sunley and E. Iglesia, *Angew. Chem., Int. Ed.*, 2006, **45**, 1617–1620.
111 A. Bhan, A. D. Allian, G. J. Sunley, D. J. Law and E. Iglesia, *J. Am. Chem. Soc.*, 2007, **129**, 4919–4924.
112 P. Cheung, A. Bhan, G. J. Sunley, D. J. Law and E. Iglesia, *J. Catal.*, 2007, **245**, 110–123.
113 H. Zhou, W. Zhu, L. Shi, H. Liu, S. Liu, Y. Ni, Y. Liu, Y. He, S. Xu, L. Li and Z. Liu, *J. Mol. Catal. A: Chem.*, 2016, **417**, 1–9.
114 E. Zhan, Z. Xiong and W. Shen, *J. Energy Chem.*, 2019, **36**, 51–63.
115 Y. Li, S. Huang, Z. Cheng, K. Cai, L. Li, E. Milan, J. Lv, Y. Wang, Q. Sun and X. Ma, *Appl. Catal., B*, 2019, **256**, 117777.
116 J. Bao, G. Yang, Y. Yoneyama and N. Tsubaki, *ACS Catal.*, 2019, **9**, 3026–3053.
117 Z. Xiong, G. Qi, E. Zhan, Y. Chu, J. Xu, J. Wei, N. Ta, A. Hao, Y. Zhou, F. Deng and W. Shen, *Chem*, 2023, **9**, 76–92.
118 J. Liu, H. Xue, X. Huang, P.-H. Wu, S.-J. Huang, S.-B. Liu and W. Shen, *Chin. J. Catal.*, 2010, **31**, 729–738.
119 K. Cao, D. Fan, L. Li, B. Fan, L. Wang, D. Zhu, Q. Wang, P. Tian and Z. Liu, *ACS Catal.*, 2020, **10**, 3372–3380.
120 R. Liu, B. Fan, W. Zhang, L. Wang, L. Qi, Y. Wang, S. Xu, Z. Yu, Y. Wei and Z. Liu, *Angew. Chem., Int. Ed.*, 2022, **61**, e202116990.
121 R. Liu, B. Fan, Y. Zhi, C. Liu, S. Xu, Z. Yu and Z. Liu, *Angew. Chem., Int. Ed.*, 2022, **61**, e202210658.
122 Y. Sun, P. Gao, Y. Ji, K. Chen and G. Hou, *ACS Catal.*, 2024, **14**, 1494–1504.
123 W. Rachmady and M. A. Vannice, *J. Catal.*, 2002, **209**, 87–98.
124 H. Olcay, Y. Xu and G. W. Huber, *Green Chem.*, 2014, **16**, 911–924.
125 J. Shangguan, M. V. Olarte and Y.-H. Chin, *J. Catal.*, 2016, **340**, 107–121.
126 M. Zhang, J. Du and Y. Chen, *Catal. Sci. Technol.*, 2023, **13**, 1345–1357.
127 X. Dong, J. Tian, J. Lei and Y. Chen, *J. Environ. Chem. Eng.*, 2022, **10**, 107517.
128 M. Zhang, R. Yao, H. Jiang, G. Li and Y. Chen, *RSC Adv.*, 2017, **7**, 1443–1452.
129 X. Dong, J. Lei, Y. Chen, H. Jiang and M. Zhang, *Appl. Catal., B*, 2019, **244**, 448–458.
130 Y. Zhao, T. Nishida, E. Minami, S. Saka and H. Kawamoto, *Energy Rep.*, 2020, **6**, 2249–2255.
131 Y. Chen, Z. Zhai, J. Liu, J. Zhang, Z. Geng and H. Lyu, *Phys. Chem. Chem. Phys.*, 2020, **22**, 7564–7576.
132 Y. Wang, Y. Shen, Y. Zhao, J. Lv, S. Wang and X. Ma, *ACS Catal.*, 2015, **5**, 6200–6208.
133 C.-L. Ye, C.-L. Guo and J.-L. Zhang, *Fuel Process. Technol.*, 2016, **143**, 219–224.
134 H. Sheng, H. Zhang, H. Ma, W. Qian and W. Ying, *Catal. Today*, 2020, **358**, 122–128.
135 M. Wu, X. Hou, Y. Quan, J. Zhao and J. Ren, *ChemistrySelect*, 2020, **5**, 11517–11521.
136 Y. Xi, Y. Hai, D. Yao, A. Li, W. Yang, J. Lv, Y. Wang and X. Ma, *Mol. Catal.*, 2022, **532**, 112708.
137 F. Zhang, Z. Chen, X. Fang, H. Liu, Y. Liu and W. Zhu, *J. Energy Chem.*, 2021, **61**, 203–209.
138 D. Wang, G. Yang, Q. Ma, M. Wu, Y. Tan, Y. Yoneyama and N. Tsubaki, *ACS Catal.*, 2012, **2**, 1958–1966.
139 A. Li, D. Yao, Y. Yang, W. Yang, Z. Li, J. Lv, S. Huang, Y. Wang and X. Ma, *ACS Catal.*, 2022, **12**, 1315–1325.
140 Y. Wang, J. Liao, J. Zhang, S. Wang, Y. Zhao and X. Ma, *AIChE J.*, 2017, **63**, 2839–2849.
141 W. Zhou, J. Kang, K. Cheng, S. He, J. Shi, C. Zhou, Q. Zhang, J. Chen, L. Peng, M. Chen and Y. Wang, *Angew. Chem., Int. Ed.*, 2018, **57**, 12012–12016.
142 J. Kang, S. He, W. Zhou, Z. Shen, Y. Li, M. Chen, Q. Zhang and Y. Wang, *Nat. Commun.*, 2020, **11**, 827.
143 F. Zhang, K. Chen, Q. Jiang, S. He, Q. Chen, Z. Liu, J. Kang, Q. Zhang and Y. Wang, *ACS Catal.*, 2022, **12**, 8451–8461.
144 S. Han, D. Fan, N. Chen, W. Cui, L. He, P. Tian and Z. Liu, *ACS Catal.*, 2023, **13**, 10651–10660.
145 X. Xu, Y. Liu, F. Zhang, W. Di and Y. Zhang, *Catal. Today*, 2017, **298**, 61–68.
146 J. Li and W. Cheng, *Appl. Energy*, 2020, **277**, 115574.
147 M. Aresta, A. Dibenedetto and A. Angelini, *Chem. Rev.*, 2014, **114**, 1709–1742.
148 X. Li, J. Ke, R. Li, P. Li, Q. Ma and T.-S. Zhao, *Chem. Eng. Sci.*, 2023, **282**, 119226.
149 S. S. Ali, S. S. Ali and N. Tabassum, *J. Environ. Chem. Eng.*, 2022, **10**, 106962.
150 H. Kurakata, Y. Izumi and K.-i. Aika, *Chem. Commun.*, 1996, 389–390, DOI: **10.1039/CC9960000389**.
151 H. Kusama, K. Okabe, K. Sayama and H. Arakawa, *Catal. Today*, 1996, **28**, 261–266.
152 C. Yang, R. Mu, G. Wang, J. Song, H. Tian, Z.-J. Zhao and J. Gong, *Chem. Sci.*, 2019, **10**, 3161–3167.

153 K. Zheng, Y. Li, B. Liu, F. Jiang, Y. Xu and X. Liu, *Angew. Chem., Int. Ed.*, 2022, **61**, e202210991.
154 K. Zheng, Y. Li, B. Liu, J. Chen, Y. Xu, Z. Li and X. Liu, *Appl. Catal., B*, 2024, **346**, 123730.
155 L. Wang, L. Wang, J. Zhang, X. Liu, H. Wang, W. Zhang, Q. Yang, J. Ma, X. Dong, S. J. Yoo, J.-G. Kim, X. Meng and F.-S. Xiao, *Angew. Chem., Int. Ed.*, 2018, **57**, 6104–6108.
156 L. Wang, S. He, L. Wang, Y. Lei, X. Meng and F.-S. Xiao, *ACS Catal.*, 2019, **9**, 11335–11340.
157 S. Liu, C. Yang, S. Zha, D. Sharapa, F. Studt, Z.-J. Zhao and J. Gong, *Angew. Chem., Int. Ed.*, 2022, **61**, e202109027.
158 J.-n. Zheng, K. An, J.-m. Wang, J. Li and Y. Liu, *J. Fuel Chem. Technol.*, 2019, **47**, 697–708.
159 S. Zhang, X. Liu, Z. Shao, H. Wang and Y. Sun, *J. Catal.*, 2020, **382**, 86–96.
160 K. An, S. Zhang, H. Wang, N. Li, Z. Zhang and Y. Liu, *Chem. Eng. J.*, 2022, **433**, 134606.
161 G. Luo, Z. Li, Q. Liu, S. Guo, X. Pei, J. Lv, S. Huang, Y. Wang and X. Ma, *Chem. Eng. J.*, 2023, **475**, 146206.
162 B. An, Z. Li, Y. Song, J. Zhang, L. Zeng, C. Wang and W. Lin, *Nat. Catal.*, 2019, **2**, 709–717.
163 L. Ding, T. Shi, J. Gu, Y. Cui, Z. Zhang, C. Yang, T. Chen, M. Lin, P. Wang, N. Xue, L. Peng, X. Guo, Y. Zhu, Z. Chen and W. Ding, *Chem*, 2020, **6**, 2673–2689.
164 D. Xu, M. Ding, X. Hong, G. Liu and S. C. E. Tsang, *ACS Catal.*, 2020, **10**, 5250–5260.
165 X. Wang, P. J. Ramírez, W. Liao, J. A. Rodriguez and P. Liu, *J. Am. Chem. Soc.*, 2021, **143**, 13103–13112.
166 S. Bai, Q. Shao, P. Wang, Q. Dai, X. Wang and X. Huang, *J. Am. Chem. Soc.*, 2017, **139**, 6827–6830.
167 J. Chen, Y. Zha, B. Liu, Y. Li, Y. Xu and X. Liu, *ACS Catal.*, 2023, **13**, 7110–7121.
168 D. Wang, Q. Bi, G. Yin, W. Zhao, F. Huang, X. Xie and M. Jiang, *Chem. Commun.*, 2016, **52**, 14226–14229.
169 D. Yang, W. Pei, S. Zhou, J. Zhao, W. Ding and Y. Zhu, *Angew. Chem., Int. Ed.*, 2020, **59**, 1919–1924.
170 X. Ye, C. Yang, X. Pan, J. Ma, Y. Zhang, Y. Ren, X. Liu, L. Li and Y. Huang, *J. Am. Chem. Soc.*, 2020, **142**, 19001–19005.
171 J. Zhang, Q. Qian, M. Cui, C. Chen, S. Liu and B. Han, *Green Chem.*, 2017, **19**, 4396–4401.
172 Q. Qian, M. Cui, J. Zhang, J. Xiang, J. Song, G. Yang and B. Han, *Green Chem.*, 2018, **20**, 206–213.
173 Y. Wang, J. Zhang, Q. Qian, B. B. Asare Bediako, M. Cui, G. Yang, J. Yan and B. Han, *Green Chem.*, 2019, **21**, 589–596.
174 B. B. Asare Bediako, Q. Qian, J. Zhang, Y. Wang, X. Shen, J. Shi, M. Cui, G. Yang, Z. Wang, S. Tong and B. Han, *Green Chem.*, 2019, **21**, 4152–4158.
175 Y. Weng, X. Wang and Y. Zhang, *Trends Chem.*, 2022, **4**, 374–377.
176 X. Zhuang, H. Wang, S. Jiang, X. Hu, T. Su, X. Zhang and L. Ma, *Green Chem. Eng.*, 2023, DOI: **10.1016/j.gce.2023.08.002**.
177 N. Ji, T. Zhang, M. Zheng, A. Wang, H. Wang, X. Wang and J. G. Chen, *Angew. Chem., Int. Ed.*, 2008, **47**, 8510–8513.
178 A. Wang and T. Zhang, *Acc. Chem. Res.*, 2013, **46**, 1377.
179 J. Pang, M. Zheng, R. Sun, A. Wang, X. Wang and T. Zhang, *Green Chem.*, 2016, **18**, 342–359.
180 M. Zheng, J. Pang, R. Sun, A. Wang and T. Zhang, *ACS Catal.*, 2017, **7**, 1939–1954.
181 G. Xu, A. Wang, J. Pang, X. Zhao, J. Xu, N. Lei, J. Wang, M. Zheng, J. Yin and T. Zhang, *ChemSusChem*, 2017, **10**, 1390–1394.
182 C. Yang, Z. Miao, F. Zhang, L. Li, Y. Liu, A. Wang and T. Zhang, *Green Chem.*, 2018, **20**, 2142–2150.
183 M. Yang, H. Qi, F. Liu, Y. Ren, X. Pan, L. Zhang, X. Liu, H. Wang, J. Pang, M. Zheng, A. Wang and T. Zhang, *Joule*, 2019, **3**, 1937–1948.
184 H. Song, P. Wang, S. Li, W. Deng, Y. Li, Q. Zhang and Y. Wang, *Chem. Commun.*, 2019, **55**, 4303–4306.
185 C. Li, G. Xu, C. Wang, L. Ma, Y. Qiao, Y. Zhang and Y. Fu, *Green Chem.*, 2019, **21**, 2234–2239.
186 Q. Liu, H. Wang, H. Xin, C. Wang, L. Yan, Y. Wang, Q. Zhang, X. Zhang, Y. Xu, G. W. Huber and L. Ma, *ChemSusChem*, 2019, **12**, 3977–3987.
187 H. Xin, H. Wang, S. Li, X. Hu, C. Wang, L. Ma and Q. Liu, *Sustainable Energy Fuels*, 2022, **6**, 2602–2612.
188 H. Xin, H. Wang, X. Hu, X. Zhuang, L. Yan, C. Wang, L. Ma and Q. Liu, *React. Chem. Eng.*, 2023, **8**, 64–76.
189 D. Chu, Y. Xin and C. Zhao, *Chin. J. Catal.*, 2021, **42**, 844–854.
190 D. Chu, Z. Luo, Y. Xin, C. Jiang, S. Gao, Z. Wang and C. Zhao, *Fuel*, 2021, **292**, 120311.
191 Y. Wu, C. Dong, H. Wang, J. Peng, Y. Li, C. Samart and M. Ding, *ACS Sustainable Chem. Eng.*, 2022, **10**, 2802–2810.
192 Y. Weng, Y. Wang, M. Zhang, X. Wang, Q. Sun, S. Mu, H. Wang, M. Fan and Y. Zhang, *Catal. Today*, 2023, **407**, 89–95.
193 B. Gumina, C. Espro, S. Galvagno, R. Pietropaolo and F. Mauriello, *ACS Omega*, 2019, **4**, 352–357.
194 J. Pang, J. Sun, M. Zheng, H. Li, Y. Wang and T. Zhang, *Appl. Catal., B*, 2019, **254**, 510–522.
195 J. Huo, J.-P. Tessonnier and B. H. Shanks, *ACS Catal.*, 2021, **11**, 5248–5270.
196 J. Pang, A. Wang, M. Zheng, Y. Zhang, Y. Huang, X. Chen and T. Zhang, *Green Chem.*, 2012, **14**, 614–617.
197 M. Besson, P. Gallezot and C. Pinel, *Chem. Rev.*, 2014, **114**, 1827–1870.
198 W. Liu, Y. Chen, H. Qi, L. Zhang, W. Yan, X. Liu, X. Yang, S. Miao, W. Wang, C. Liu, A. Wang, J. Li and T. Zhang, *Angew. Chem., Int. Ed.*, 2018, **57**, 7071–7075.
199 L. Chen, G. Msigwa, M. Yang, A. I. Osman, S. Fawzy, D. W. Rooney and P.-S. Yap, *Environ. Chem. Lett.*, 2022, **20**, 2277–2310.
200 K. Liang, M. Wang, C. Gao, B. Dong, C. Feng, X. Zhou and J. Liu, *Sustainable Energy Technologies and Assessments*, 2021, **46**, 101319.
201 K. Afridi, *Nat. Electron.*, 2022, **5**, 62–64.
202 A. Parikh, M. Shah and M. Prajapati, *Environ. Sci. Pollut. Res.*, 2023, **30**, 57236–57252.

203 E. V. Makshina, M. Dusselier, W. Janssens, J. Degreve, P. A. Jacobs and B. F. Sels, *Chem. Soc. Rev.*, 2014, **43**, 7917–7953.
204 X. Wu, G. Fang, Y. Tong, D. Jiang, Z. Liang, W. Leng, L. Liu, P. Tu, H. Wang, J. Ni and X. Li, *ChemSusChem*, 2018, **11**, 71–85.
205 J. Pang, M. Zheng and T. Zhang, in *Adv. Catal*, ed. C. Song, Academic Press, 2019, vol. 64, pp. 89–191.
206 N. M. Eagan, M. D. Kumbhalkar, J. S. Buchanan, J. A. Dumesic and G. W. Huber, *Nat. Rev. Chem.*, 2019, **3**, 223–249.
207 J. Pang, M. Yin, P. Wu, X. Li, H. Li, M. Zheng and T. Zhang, *Green Chem.*, 2021, **23**, 7902–7916.
208 J. Zhang, E. Yoo, B. H. Davison, D. Liu, J. A. Schaidle, L. Tao and Z. Li, *Green Chem.*, 2021, **23**, 9534–9548.
209 Z. Wang, M. Yin, J. Pang, X. Li, Y. Xing, Y. Su, S. Liu, X. Liu, P. Wu, M. Zheng and T. Zhang, *J. Energy Chem.*, 2022, **72**, 306–317.
210 L. He, B.-C. Zhou, D.-H. Sun, W.-C. Li, W.-L. Lv, J. Wang, Y.-Q. Liang and A.-H. Lu, *ACS Catal.*, 2023, **13**, 11291–11304.
211 M. Yin, J. Pang, J. Guo, X. Li, Y. Zhao, P. Wu and M. Zheng, *Green Energy Environ.*, 2023, DOI: **10.1016/j.gee.2023.10.001**.
212 A. Haynes, P. M. Maitlis, G. E. Morris, G. J. Sunley, H. Adams, P. W. Badger, C. M. Bowers, D. B. Cook, P. I. P. Elliott, T. Ghaffar, H. Green, T. R. Griffin, M. Payne, J. M. Pearson, M. J. Taylor, P. W. Vickers and R. J. Watt, *J. Am. Chem. Soc.*, 2004, **126**, 2847–2861.
213 L. Lin, X. Han, B. Han and S. Yang, *Chem. Soc. Rev.*, 2021, **50**, 11270–11292.
214 B. W. J. Chen, L. Xu and M. Mavrikakis, *Chem. Rev.*, 2021, **121**, 1007–1048.
215 S. Karimi, R. R. Karri, M. Tavakkoli Yaraki and J. R. Koduru, *Environ. Chem. Lett.*, 2021, **19**, 2873–2890.
216 M. H. Barecka, P. Ds Dameni, M. Zakir Muhamad, J. W. Ager and A. A. Lapkin, *ACS Energy Lett.*, 2023, **8**, 3214–3220.
217 L.-H. Xu, S.-H. Li, H. Mao, Y. Li, A.-S. Zhang, S. Wang, W.-M. Liu, J. Lv, T. Wang, W.-W. Cai, L. Sang, W.-W. Xie, C. Pei, Z.-Z. Li, Y.-N. Feng and Z.-P. Zhao, *Science*, 2022, **378**, 308–313.
218 L. Petrus and M. A. Noordermeer, *Green Chem.*, 2006, **8**, 861–867.
219 K. Goransson, U. Soderlind, J. He and W. Zhang, *Renewable Sustainable Energy Rev.*, 2011, **15**, 482–492.
220 Y. Chung, I. Hwang, Y.-K. Yeo, O.-S. Joo and K.-D. Jung, *Korean Chem. Eng. Res.*, 2006, **44**, 323–327.
221 D. Mu, T. Seager, P. S. Rao and F. Zhao, *Environ. Manage.*, 2010, **46**, 565–578.
222 J. C. d. C. Miranda, G. H. S. F. Ponce, H. Arellano-Garcia, R. Maciel Filho and M. R. Wolf Maciel, *J. Cleaner Prod.*, 2020, **269**, 122078.
223 L. Zeng, Z. Wang, Y. Wang, J. Wang, Y. Guo, H. Hu, X. He, C. Wang and W. Lin, *J. Am. Chem. Soc.*, 2020, **142**, 75–79.
224 M. Liu, Y. Wang, X. Kong, R. T. Rashid, S. Chu, C.-C. Li, Z. Hearne, H. Guo, Z. Mi and C.-J. Li, *Chem*, 2019, **5**, 858–867.
225 H. Xu, D. Rebollar, H. He, L. Chong, Y. Liu, C. Liu, C.-J. Sun, T. Li, J. V. Muntean, R. E. Winans, D.-J. Liu and T. Xu, *Nat. Energy*, 2020, **5**, 623–632.
226 C. Guo, Y. Guo, Y. Shi, X. Lan, Y. Wang, Y. Yu and B. Zhang, *Angew. Chem., Int. Ed.*, 2022, **61**, e202205909.
227 H. Wang, X. Bi, Y. Yan, Y. Zhao, Z. Yang, H. Ning and M. Wu, *Adv. Funct. Mater.*, 2023, **33**, 2214946.
228 R. Wei, Y. Liu, H. Ma, X. Ma and Y. Yang, *J. Energy Chem.*, 2023, **86**, 23–31.
229 J. Ding, H. Bin Yang, X.-L. Ma, S. Liu, W. Liu, Q. Mao, Y. Huang, J. Li, T. Zhang and B. Liu, *Nat. Energy*, 2023, **8**, 1386–1394.
230 U. Mondal and G. D. Yadav, *Green Chem.*, 2021, **23**, 8361–8405.
231 D. W. Stephan, *Nature*, 2013, **495**, 54–55.
232 C. F. Shih, T. Zhang, J. Li and C. Bai, *Joule*, 2018, **2**, 1925–1949.

